UC Irvine
UC Irvine Previously Published Works

Title

Experimental evaluation of seismic performance of interior RC beam-column joints strengthened with FRP composites

Permalink

https://escholarship.org/uc/item/89q3j5hj

Authors

Allam, Khaled
Mosallam, Ayman S
Salama, Mohamed A

Publication Date

2019-10-01

DOI

10.1016/j.engstruct.2019.109308

Peer reviewed
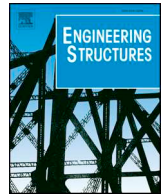
Experimental evaluation of seismic performance of interior RC beam-column joints strengthened with FRP composites

Khaled Allam[a], Ayman S. Mosallam[b,*], Mohamed A. Salama[c]

[a] *Moffatt & Nichol, Irvine, CA, USA*
[b] *University of California, Irvine, Irvine, CA, USA*
[c] *Helwan University, Cairo, Egypt*

ARTICLE INFO

ABSTRACT

Lack of joint confinement for the majority of pre-1970 reinforced concrete (RC) frame construction has resulted in weakening the link between the column and the beam and collapse of the whole structure. The main focus of this research study is based on four interrelated tasks: (i) design and development of innovative repair and retrofit techniques for reinforced concrete (RC) beam-column joints using advanced FRP composite laminates and pre-cured composite connectors; (ii) experimental evaluation of the different techniques using full-scale testing; (iii) comparison in behavior between as-built and different retrofit specimens; and (iv) conclusions and recommendations for future research.

Experimental results confirmed the superiority and success of the proposed strengthening protocols, not only in restoring the original strength capacity, but also in enhancing the overall seismic performance of the deficient joints evaluated in this study including strength and ductility. For example, the use of carbon/epoxy wet layup composite laminates resulted in an appreciable increase of both strength and ductility up to 1.34 and 3.04 times, as compared with as-built specimen, respectively. Also, the proposed technique for enhancing shear strength and rebar bond slippage of the joints using high-strength carbon/epoxy FRP composite laminates and a hybrid composite connectors (HCC) achieved significant results. The novel proposed technique improved the shear strength of the joint 2.5 times the control deficient specimen. The use of the hybrid composite connector (HCC) succeeded in relocating the hinging mechanism to form in the beam span away from the joint region. The ductility of the retrofitted specimen was 2.18 times the control (as-built) specimen. It is anticipated that the results of this pioneering study will provide alternative innovative reinforcing and strengthening methodologies to enhance the construction and repair methods for reinforced concrete moment frame structures. These innovative techniques contribute to higher reliability and safety, as well as lower construction and repair costs of RC moment frame structures. It is also anticipated that the proposed strengthening protocol can also be applied to cover similar details such as base-column, pile-cap as well as T- and knee bridge joints.

1. Introduction

Prior to 1970, the majority of constructed RC frame buildings have deficient beam-column joints due to the absence of design code requirements for transverse steel reinforcement at the joint locations (refer to Fig. 1. Among other factors, failure of a building structure is mainly due to inadequate beam-column joint strength. Failure modes observed and reported from past earthquakes indicated that these deficient details resulted in insufficient joint shear strength and/or buckling of the column's longitudinal rebars instead of forming the desired plastic hinge at the beam section. Another major contributor to failure of the majority of the beam-column joints is the adoption of

what called "strong beam/weak column" philosophy that existed in 1960's and 1970s [1]. Many studies have elaborated the need for a retrofit scheme to these deficient joints. The design guidelines for reinforced concrete beam-column joints were first published in 1976 [2]. The current American Concrete Institute [3] mandates the adoption of weak beam-strong column philosophy. This code requirement ensures the formation of the potential plastic hinge at the beam span as well as yielding of the beam longitudinal reinforcement instead of exhibiting catastrophic brittle joint shear failure.

In the past few years, several research studies that have been published focused mainly on enhancing both shear and bond strength of RC beam-column joints. Some examples of the retrofit technique included

---

* Corresponding author.
E-mail address: mosallam@uci.edu (A.S. Mosallam).

Fig. 1. Examples of damages and collapse of pre-1970s exterior and interior RC beam-column joints during past earthquakes.

epoxy injection repair, concrete jacketing, steel jacketing, addition of external steel and/or fiber reinforced polymeric (FRP) laminates. The use of epoxy injection repair technique is not acceptable method in high seismic regions due to the poor performance of epoxy when subjected to a reversed cyclic loading. Reinforced concrete and steel jacketing have been the popular choices in areas with high seismicity, especially for RC columns applications. However, these processes are labor intensive and may be considered impractical in some cases as in case of interior joints with beams in two orthogonal directions. In the late 1990s, research efforts focused on developing alternative FRP composites technique in the form of epoxy-bonded flexible laminates. Some of the attractive features of FRP composites include high strength-to-weight ratios (specific strength), higher corrosion resistance and ease of application. The main focus of this research paper is to develop and evaluate experimentally, the seismic behavior of RC beam-column joints reinforced externally with innovative fiber reinforced polymeric (FRP) composite elements. The innovative reinforcement systems are designed specifically to overcome two common joint deficiencies, namely shear and bond-slip. Analytical and numerical models for the proposed techniques are described by Mosallam et al. [4].

The two major sources of joint deficiencies of existing RC buildings are [5]: *(i) lack of column confinement at the beam-column joint region, and (ii) inadequate anchorage of the beam's bottom reinforcement (bond-slip deficiency)*. The majority of past published research work has focused on the repair and retrofit of the beam-column exterior joints using either conventional materials or off-the-shelf polymeric composites. In this study, innovative externally strengthening techniques for reinforcing interior RC beam-column joints are investigated. Some of the techniques that are evaluated for the first time in this study include the use of ultra-high modulus carbon fibers [$E_1 = 6.2 \times 10^5$ MPa (92.0×10^6 psi)], and hybrid composite connectors (HCC). For repair and external strengthening applications, three systems are evaluated including high-strength carbon/epoxy composite laminates, high-modulus carbon/epoxy laminates, and E-glass/epoxy external laminates. For bond-slip retrofit, the light-weight hybrid composite connector (refer to Fig. 2, developed by the second author, is evaluated through large-scale tests. The hybrid composite connectors (HCC) are attached to both column and beams sides using both high-strength bolts and high-strength epoxy adhesives. All external FRP laminates are instrumented with calibrated strain gauges, potentiometers, and linear variable differential transducers (LVDT's) for continuous and accurate measurements of strain distribution at different critical locations. Data were automatically collected via a calibrated computerized data acquisition system.

2. Related research

Several studies were developed to study the behavior of reinforced concrete beam-column joints. Paulay, Park and Priestley [6] studied the beam-column joints under seismic actions. Hakuto, Park and Tanaka [7] have studied the seismic performance of both interior and exterior beam-column joints with substandard reinforcing details. Many other studies were conducted as Hanson and Connor [8], Corazao and Durrani [9], Fujii and Morita [10], Aycardi et al. [11], Beres et al. [12], Choudhuri et al. [13], Bracci et al. [14], Cosenza and Manfredi [15], Kurose et al. [16] and Walker [17].

During the last few decades, research studies were conducted to upgrade and retrofit the deficient RC beam-column joint. Different retrofit schemes such as concrete and steel jacketing were conducted by Corazao and Durrani [9], and Prison and Baraka [18]. Appa Roa et al. [19] studied the performance of non-seismically designed RC beam-column joints strengthened by various schemes subjected to seismic loads. Biddah et al. [20] proposed a new strengthening technique for exterior joint with a corrugated steel jacket around the column.

With the introduction of the FRP composites bridge columns rehabilitation in the early 1990s, this new technique was extended to strengthen seismically-deficient beam-column joints. A pioneering study introducing the use of composites for strengthening beam-column joints was reported by Mosallam [21]. A comprehensive report on application of FRP composites in construction is presented by Mosallam [22] and Mosallam et al. [23]. Mukherjee and Joshi [24] studied FRPC reinforced concrete beam-column joints under cyclic excitation. Antonopoulos and Triantafillou [25] conducted an experimental research on 18 exterior 2/3 scale joints strengthened with different configurations of pultruded carbon strips, FRP carbon/ and E-glass/epoxy laminates. Ayala et al. [26] conducted a study on using of FRP fabric for strengthening of reinforced concrete beam-column joints. Mahini and Ronagh [27] conducted a research study on retrofitted RC exterior beam-column joints with CFRP under cyclic loads. Shannag and Abu-Dyya [28] studied the lateral load response of high-performance fiber reinforced concrete beam-column joints. Liu [29] studied the seismic behavior of beam-column joint assemblies reinforced with steel fibers. Tsonos [30] studied the effect of CFRP jackets on retrofitting beam-column subassemblies. Supaviriyakit and Pimanmas [31] conducted a study to compare the performance of a substandard beam-column joint with and without initial bond between beam longitudinal rebars and concrete in the joint core. Le-Trung et al. [32] reported results of an experimental study on eight RC beam–column joints strengthened using CFRP composites. Different CFRP laminates configurations were assessed including T-, L-, and X-shapes. Ma et al. [33] reported the results of a study that focused on seismic retrofit of full-scale RC interior beam-column-slab strengthened with CFRP laminates. Lately, Esmaeeli et al. [34] proposed a hybrid steel/composites retrofit system for seismic strengthening of shear-deficient corner RC beam-column joints. Danesh et al. [35] studied the effectiveness of GFRP layers for joint strengthening of two-way corner beam-column connection. Mosallam [36]
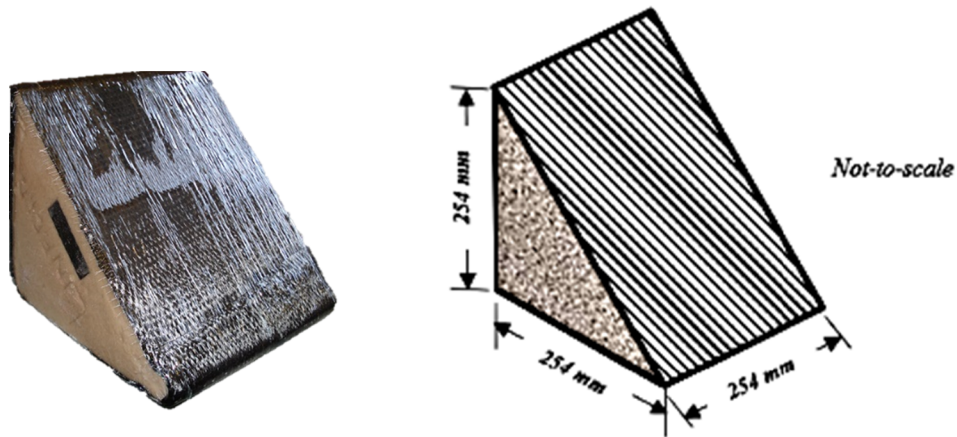
Fig. 2. The Hybrid Composite Connector (HCC).

conducted a research study on structural performance of reinforced concrete column-tie beam assembly retrofitted with FRP composites.

3. Experimental program

Eight full-scale interior RC beam-column specimens were evaluated that mimic the interior beam-column joint part between two stories at a reinforced concrete building. The specimens were tested by applying both gravity and low-frequency full cyclic load on a sub-assembly of interior reinforced concrete (RC) beam-column joint except control specimen (AB-1) that was tested under dynamic impulse loading resembling the near-fault effect during an earthquake event. The sub-assemblage shown in Fig. 3 represents a typical interior beam-column joint found in a reinforced concrete (RC) frame building isolated between two stories and two bays at the moment inflection point under lateral seismic loading. To simulate condition of zero moment at the

upper column, the top of the column is subjected to horizontal lateral force but free to rotate in-plane through the actuator released arm head. To simulate a zero-moment condition at the lower column, the bottom of the column is mounted on a steel hinge support connected to the strong floor. In order to simulate the point of contra-flexural at the mid span of the beam, the end of each beam is restrained vertically and free to rotate in-plane direction using a pinned axial support. The specimen setup considers the P-Δ effect as the whole specimen is free to rotate in the lateral loading. The boundary conditions of the test setup are presented in Fig. 4.

Seven specimens were designed and detailed following the pre-1970 construction practice based on ACI318-63 [1] (refer to Figs. 5 and 6). One specimen was designed in accordance to the current ACI318-14 code [3] (refer to Fig. 7). The experimental results of the four control (as-built) specimens were established as the baseline for comparing their hysteretic response, stiffness, load/displacement envelope and
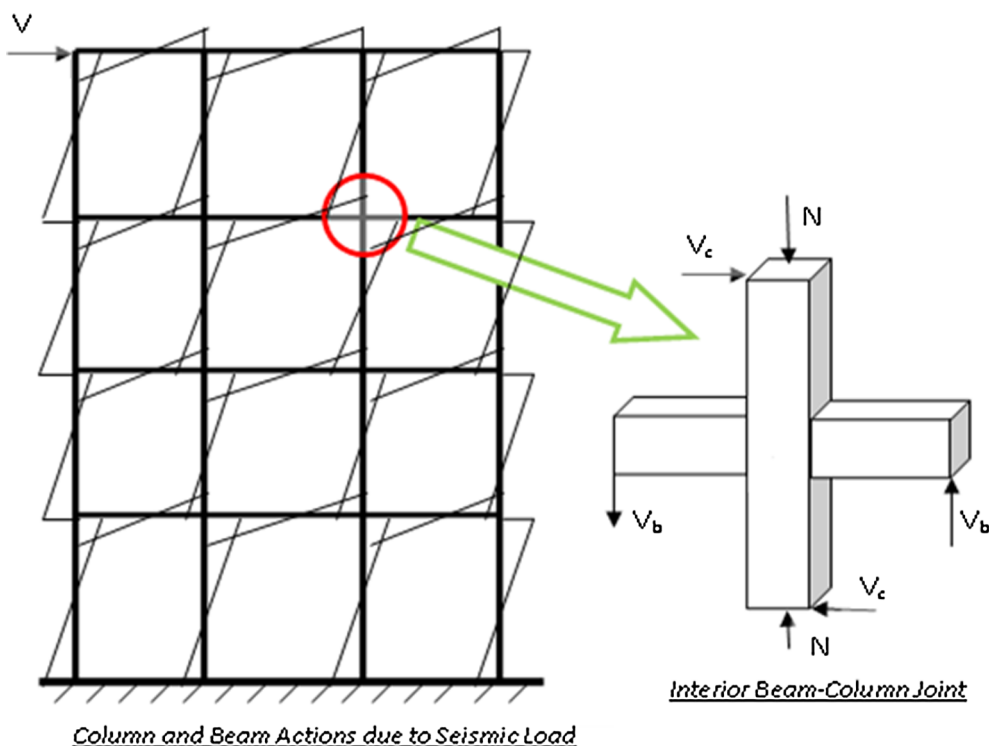

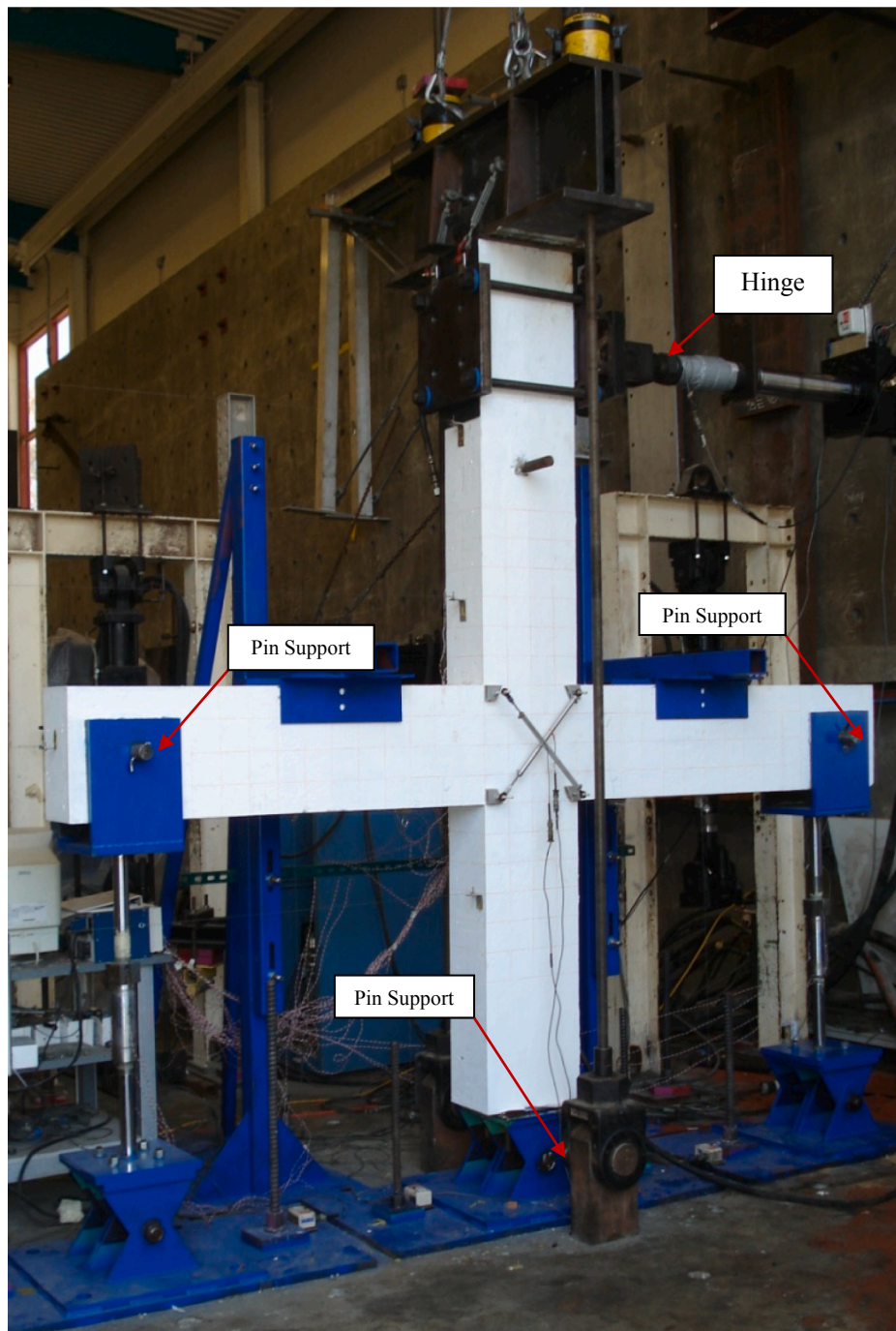**Fig. 3.** Interior beam-column joint sub-assemblage.

Fig. 4. Typical beam-column joint test setup.

total energy dissipation with those of the repaired and retrofitted joint specimens. The other four full-scale interior RC beam-column specimens with identical details as the control specimen were retrofitted with different types of FRP composite laminates. The first retrofitted specimen was rehabilitated with high-strength carbon/epoxy fiber reinforced polymer and designated as RS-SC. The second retrofitted specimen was rehabilitated with E-glass/epoxy fiber reinforced polymer and designated as RS-G. The third retrofitted specimen was rehabilitated with high-modulus carbon/epoxy reinforced polymer and designated as RS-MC. The fourth retrofitted specimen was rehabilitated with high-strength carbon fiber reinforced polymer for shear enhancement and a hybrid composite connectors (HCC) for remedying the discontinuous rebar bond slip. This specimen was designated as RS-

SCC. The aims for retrofitting these specimens are: (i) enhancement of joint shear strengthening and ductility, (ii) improvement of column confinement subjected to reversal cyclic loading, and (iii) increasing ultimate capacity of the beam against potential bottom rebars reinforcement bond slip.

3.1. Specimen design and geometry

Two different sets of deficient RC beam-column joint specimens were designed according to the 1963 ACI 318-63 code [1] and one specimen was designed according to the current ACI 318-14 code [3]. For all specimens, the dimensions of beam members were 254 mm (10 in.) × 406 mm (16 in.) reinforced with 4Φ19 mm (4#6)
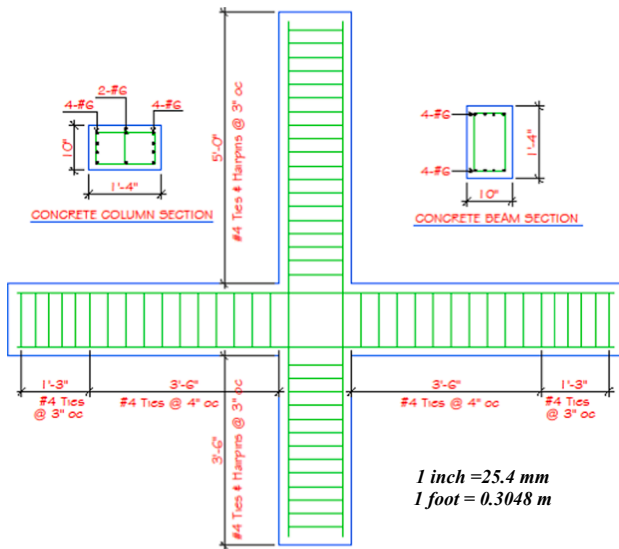
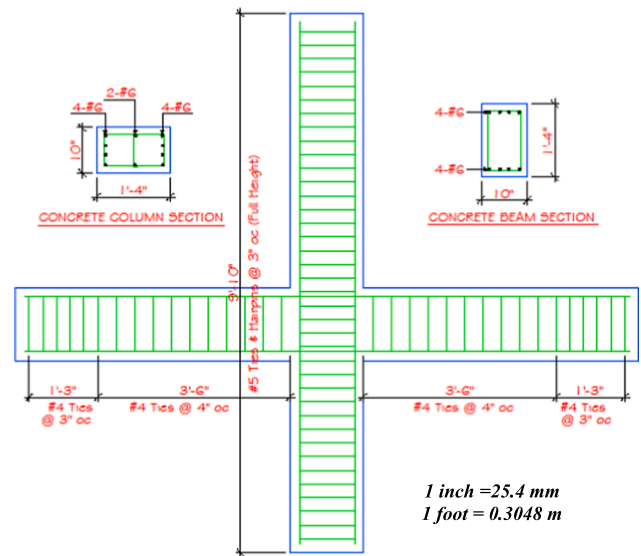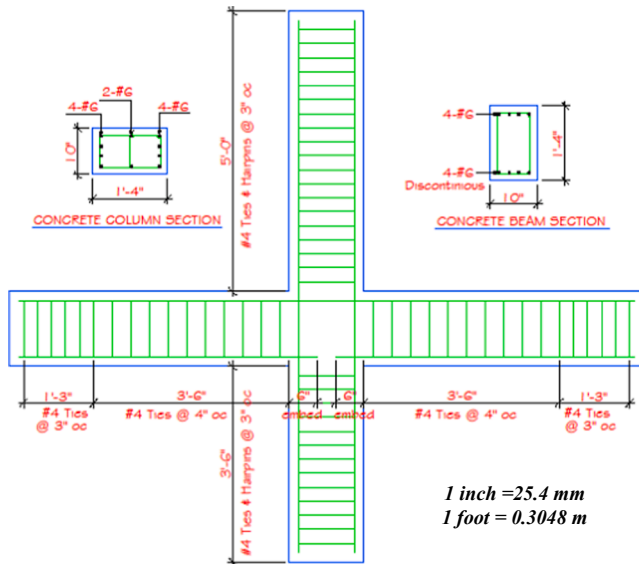**Fig. 5.** First and second deficient specimen with unconfined joint.

Fig. 6. Third deficient specimen with unconfined joint and discontinuity of Beam's bottom reinforcement rebars.

longitudinal reinforcement rebars placed at both top and bottom of beam section. The beams transverse reinforcement is in the form of 13 mm (#4) steel stirrups spaced equally at 102 mm (4 in.) on center from the face of the column to a distance of 381 mm (1 foot-3 in.) away from the beam edge and the remaining stirrups with the same diameter are positioned at 76.2 mm (3 in.) on center. For all specimens, the column dimensions are 254 mm (10 in.) × 406 mm (16 in.) with 4 Φ 19 mm (4#6) longitudinal steel rebars placed at the top and bottom constituting about 2% steel reinforcement ratio (ρ_s). The full height of the column is confined with 13 mm (# 4) stirrups spaced at 76.2 mm (3 in.) on center except at the joint region.

As stated earlier, deficient joint specimens were detailed based on the pre-1970 construction practice. The first two deficient joint specimens were detailed without the use of any confinement stirrups within the joint zone. The third deficient specimen was detailed with discontinuous beam's bottom reinforcement rebars and without confinement stirrups at the joint region. Fig. 5 presents the typical reinforcement details of the first and second deficient specimens. The steel reinforcement detail of the third deficient specimen is shown in Fig. 6.

Fig. 7. Fourth control specimen with confined joint according to ACI318-14 [3].

Finally, the fourth control (as-built) specimen was designed according to ACI-318-14 code [3] and detailed with 13 mm (# 4) stirrups equally spaced at 76 mm (3 in.) on center within the joint region. The full steel reinforcement details of the fourth control specimen is presented in Fig. 7.

3.2. Material properties

The average 28-day compressive concrete strength was 31.0 MPa (4.5 ksi) with test day strength of 34.5 MPa (5.0 ksi). All steel reinforcements used in this study were grade A615. The reinforcement tensile properties were tested according to ASTM A370. The yield stress of the reinforcement steel was 468.84 MPa (68.0) ksi with an ultimate stress of 620.53 MPa (90.0) ksi.

Three types of FRP composites repair and the retrofitting systems were assessed in this study. This included (i) E-glass/epoxy wet lay-up laminates with average volume fraction of 40%, (ii) high-strength carbon/epoxy laminates, and (iii) high-modulus carbon/epoxy laminates. For the carbon-based composites, the typical volume fraction is about 45%. All composite laminates evaluated in this study were tested according to the ASTM D3039/D3039M-17 [37] in order to determine mechanical properties of each material. The tensile strength and elastic modulus of E-glass/epoxy, high-strength carbon/epoxy, and high-modulus carbon/epoxy wet lay-up laminates are presented in Table 1. A mixture of sand and special room temperature-cured, 2-part epoxy was used to fabricate the core of the hybrid composite connector. The sand and epoxy adhesive used in fabricating the repair material were made by mixing fine sand of grade 60 with moisture tolerant, high-modulus, high-strength, two-part structural epoxy.

3.3. Test setup

The typical test setup of beam-column joint evaluated in this study is shown in Fig. 8. All interior beam-column joint specimens are tested

Table 1
FRP laminate mechanical properties.

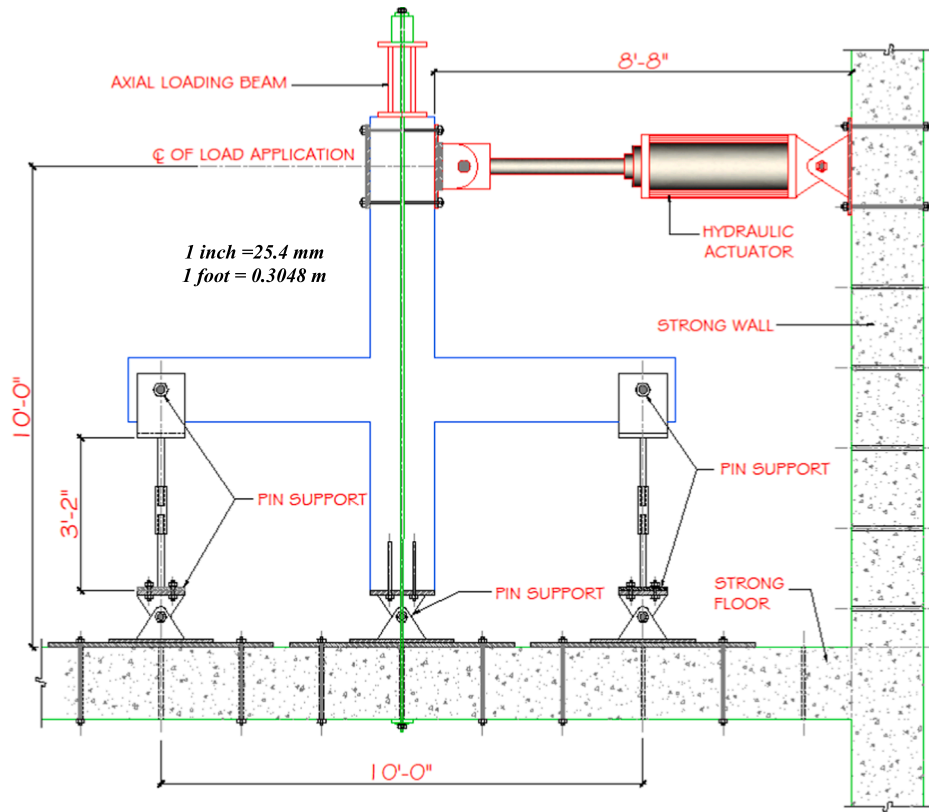| Laminate type	Ultimate strength MPa (ksi)	Modulus MPa (Msi)
FC061/RN075LPL	989.4 (143.9)	62,05 (29.0)
FE261/RN075LPL	625.4 (90.7)	26,200 (3.8)
CH41/RN075LPL	355.0 (51.5)	140,653 (20.4)

Fig. 8. Specimen test setup.

under quasi-static cyclic loading to simulate seismic load, excluding the first control specimen that is tested under dynamic impulse loading to simulate earthquake loads at near fault sites. An axial vertical load is applied on the column to simulate the effect of gravity load. Prior to applying the lateral dynamic or cyclic loading, the column is loaded with 1.0% of its axial compressive capacity according to ACI318-14 [3] requirements (i.e. $P_{gravity} = 0.1 A_g f_c'$ where A_g is the concrete cross sectional area and f_c' is the concrete compressive strength).

In order to simulate lateral earthquake loads imposed on the beam-column specimens, a 667-kN (150-kip) calibrated servo-hydraulic actuator with internal linear variable displacement transducer (LVDT) and in-line calibrated load cell is used. As mentioned earlier, the axial load is applied to the specimen via load transfer built-up steel beam placed on the top of the column to transfer the hydraulic jacks load as shown in Fig. 9. In order to prevent specimens' out-of-plane movement, guide frames are placed on each side of the specimen. Displacement generated at different critical locations are captured using four calibrated linear string potentiometers (string-pots) that were securely mounted on a metal frame placed next to the specimen that is connected to the specimen at heights of 965.0 mm (38.0 in.), 1524 mm (60 in.), 1778 mm (70 in.), and 2235 mm (88 in.) measured from the floor level. Calibrated horizontal string potentiometers are used to measure the global horizontal displacement of the specimen. Another four string-pots are installed under the beams (two below each beam) at a distance of 457.0 mm (18.0 in.) and 711.0 mm (28.0 in.) measured from the column centerline to measure the global vertical displacement of the specimen. The locations of the potentiometers for measuring horizontal deflections with respect to a fixed datum and vertical deflection with respect to the strong floor are shown in Fig. 9. A calibrated computerized data acquisition system was used to continuously record actuator force and displacement, as well as strain from the different electrical strain gauges installed on steel rebars and FRP laminates. Each specimens was instrumented with different strain gauges and linear potentiometers to monitor: (1) longitudinal rebar strain in the

top and bottom column, (2) longitudinal top and bottom rebar strain in each beam, (3) steel stirrups strain in the top and bottom column, (4) steel stirrups strain in each beam, and (5) the global specimen translation and rotation relative to reference metal frame in the horizontal direction and to the strong floor in the horizontal direction. Fig. 10 shows the locations of the strain gauges.

3.4. Load history

The loading protocol was set based on the International Code Council Evaluation Service (ICC-ES) Acceptance Criteria AC125 [38]. The typical lateral loading history used in all tests is shown in Fig. 11. Four initial, fully reversed cycles, were applied in a load-control regime, up to ¼ f_y, ½ f_y, ¾ f_y, and f_y, where f_y equal to the horizontal lateral force corresponding to first yield of the extreme longitudinal reinforcing rebar. The remainder of the test was conducted in displacement-control regime with three cycles each at displacement ductility levels of $\mu_d = 1, 1.5, 2, 3$, etc. up to failure of each specimen. The displacement ductility index is defined as

$$\mu_d = \frac{\Delta_d}{\Delta_y} \tag{1}$$

where Δ_d is the demand displacement and Δ_y is the idealized yield displacement.

The first yield of the reinforcement rebar is calculated based on moment curvature analysis of the beam and column section. When the Linear Potentiometer Transducer (LPT) records the first yield occurred to any of the steel reinforcement rebar, the corresponding displacement $\Delta'y$ measured at the specimen is used to calculate the experimental elastic bending stiffness k_e, where
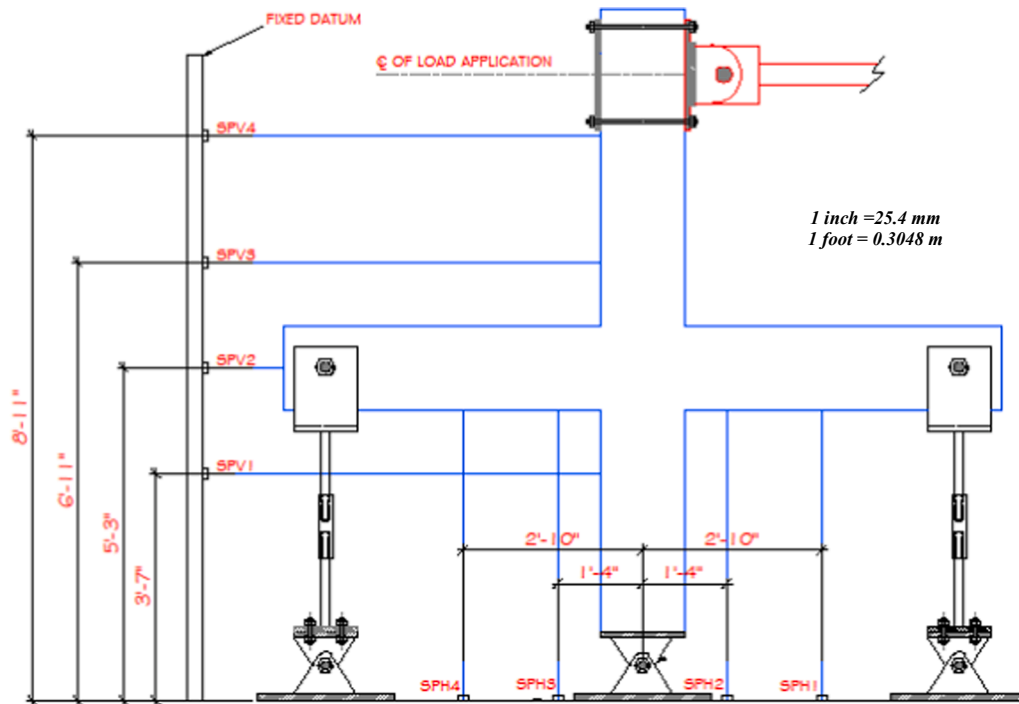
$$k_e = \frac{f_y'}{\Delta_y} \tag{2}$$

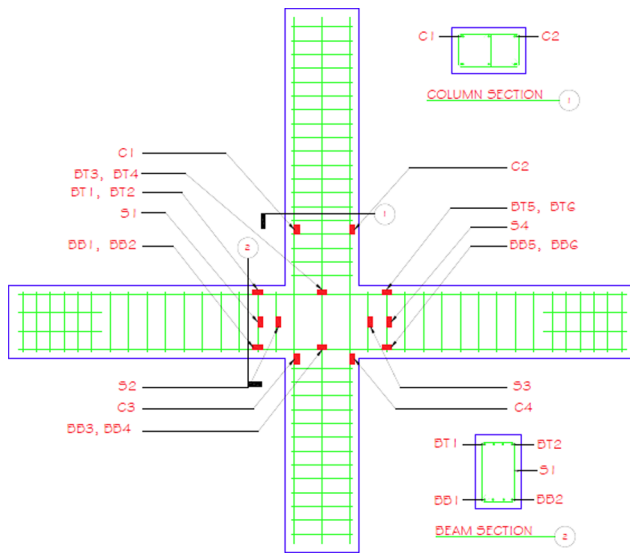**Fig. 9.** Location of horizontal and vertical displacement potentiometers.

Fig. 10. Location of strain gauges on reinforcement rebars.

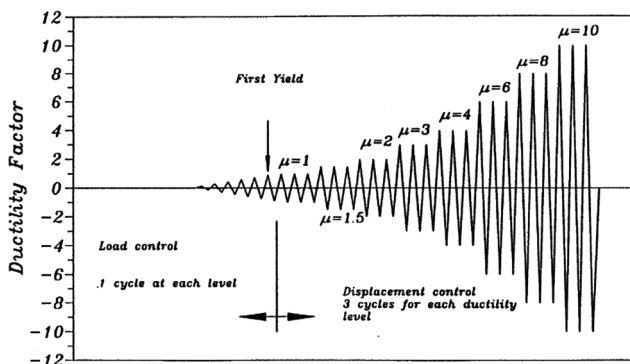
Fig. 11. Typical lateral loading history (ICC-ES AC125-17) [38].

where f_y' is the record force at a displacement $\Delta'y$.

The idealized yield force F_y in the moment-curvature analysis is computed corresponding to the force at which the extreme confined concrete compression fibers reaches $\varepsilon_c = 0.003$. The experimental elastic bending stiffness and the ideal yield force F_y are then used to calculate the idealized yield displacement Δ_y. This idealized yield displacement Δ_y is set as the yield displacement for displacement ductility $\mu_d = 1.0$.

$$\Delta = f_y/k_e \tag{3}$$

3.5. Test matrix

The experimental program is classified according to its type of deficiency/strengthens and simulated seismic loading. Eight full-scale specimens were tested in this research study. Each specimen was given a designated code to distinguish between the control (as-built), repair and the retrofit.

The deficient as-built wall specimens without any repair or retrofit and control specimen designed per current ACI318-14 code [3] were given a code "AB". The repaired specimen of a damaged as-built specimen was given a code "AR". Lastly, the retrofitted-strengthened specimens of deficient specimen pre-earthquake event were given a code "RS". The experimental test matrix is presented in Table 2.

### 3.6. Design of FRP composite system

Generally, the majority of the joint shear failures are caused due to poor reinforcement details, leading to creation of weak links in RC building frame structure. The purpose of strengthening the beam-column joint connections is to withstand joint shear force (V_j) developed due to reversal seismic loading and prevent brittle shear failure from occurring in the joint core. Fig. 12 shows the forces acting on an interior beam-column joint.

The joint shear force demand is computed as follows:

$$T_b = n(A_s f_y) = 4(283.87 \text{mm}^2 \times 468.84 \text{kPa}) = 532.36 \text{kN}(119.7 \text{kips}) \tag{4}$$

Table 2
Test matrix.

Group	Code	Specimen description	Loading pattern
Control (As-built)	AB-1	Unconfined Joint according to Pre-1970 code [1]	Dynamic
	AB-2	Unconfined Joint according to Pre-1970 code [1]	Quasi-static
	AB-3	Unconfined Joint & discontinuity of beam bottom rebar according to Pre-1970 code [1]	Quasi-static
	AB-3	Confined Joint according to ACI 318-14 code [3]	Quasi-static
Repaired	AR-2	Repaired joint with high-strength CFRP laminates	Quasi-static
Retrofit	RS-SC	Strengthened joint with high strength CFRP laminates	Quasi-static
	RS-G	Strengthened joint with GFRP laminates	Quasi-static
	RS-MC	Strengthened joint with high-modulus CFRP laminates	Quasi-static
	RS-SCC	Strengthened joint with high-strength CFRP laminates & advanced composite connectors	Quasi-static
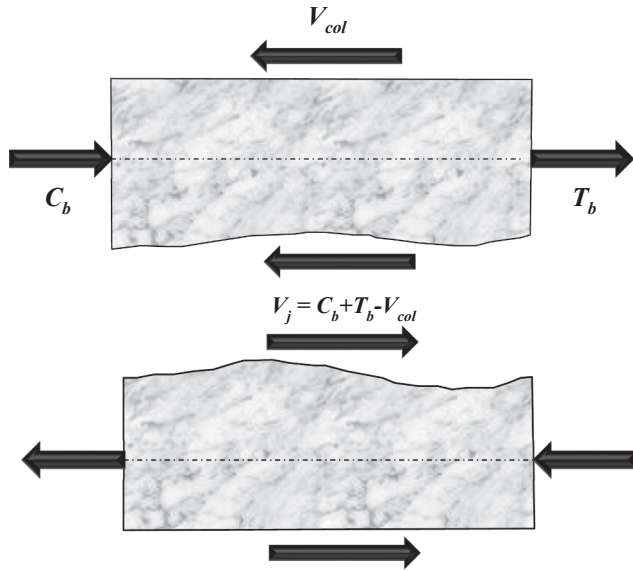
Fig. 12. A free-body diagram at mid-height of interior beam-column joint.

$$V_j = T_b + C_b - V_{col} \tag{5}$$

$$T_b = C_b = 532.36 \text{kN}(119.7 \text{kips}) \tag{6}$$

$$V_{col} = \frac{2(1.25M_{nb})}{L_c} = \frac{2(154)}{3.05} = 126.33 \text{kN}(28.4 \text{kips}) \tag{7}$$

$$V_j = 2T_b - V_{col} = 2 \times 532.36 \text{kN} - 126.33 \text{kN} = 938.57 \text{kN}(211 \text{kips}) \tag{8}$$

where T_b is the internal tension force presented in the beam section, C_b is the beam internal compression force, M_{nb} is the beam moment capacity, V_{col} = column shear force, and n = the number of reinforcing steel rebars in the beam section. The shear strength of the joint is:

$$V_j = V_c + V_s + V_{FRP} \tag{9}$$

$$V_c = 2\sqrt{f_c'} b_j d_j = 2\sqrt{5200} \times 10 \times 16 = 23.1 \text{kips}(102.75 \text{kN}) \tag{10}$$

where bj is the joint width, and dj is the joint depth.

As a conservative approach, the contribution of the concrete strength to the joint shear capacity is neglected. For the case of no ties provided in the joint, V_s is taken to be zero.

The number of FRP composite plies required to resist the horizontal joint shear, N_{FRP}, is computed as:

$$N_{FRP} = \frac{V_{FRP}}{h_j * t_{FRP} * f_{fe}} \tag{11}$$

where V_{FRP} is the horizontal shear due to FRP contribution, h_j is the height of the joint, t_{FRP} is the thickness of a unit FRP ply, and f_{fe} = the effective tensile stress per FRP composite ply. The effective tensile stress of FRP (f_{fe}) is expressed according to the ACI440.2R-08 [39] as:

$$f_{fe} = E_f \varepsilon_{fe} \tag{12}$$

where E_f is the longitudinal tensile modulus of elasticity of FRP, and ε_{fe} is the effective strain level in the FRP attained at failure. According to ACI440.2R-08 [39], the loss of concrete aggregate interlock has been observed to take place at fiber strains less than the ultimate fiber strain. In order to preclude this mode of failure, the maximum strain level in the FRP laminate is limited by 0.004.

3.7. Retrofitting laminates schedule

Prior to the application of external carbon/epoxy or E-glass/epoxy composite laminate, the required number of plies were determined according to the design described in the previous section. Based on the calculated joint shear demand, the total number of plies was applied to the joint, splitting number of plies equally on each face. A cross-angle (± 45°) plies were added to have a smooth transition in the layup orientation between the vertical and horizontal plies. Following ACI440R2-08 [39] design recommendations, two vertical composite plies were bonded to each face of the joint for improving anchorage and increasing joint shear strength. Table 3 shows the number of the number of plies in each FRP laminate and the corresponding layup sequence for each strengthened beam-column joint specimen. Figs. 13–17 show lamination layup scheme for different joint specimens evaluated in this study.

4. Analysis of test results

The following paragraphs describe the different fiber architectures and geometrical details of the composite lamination retrofitting system used for different beam-column joints.
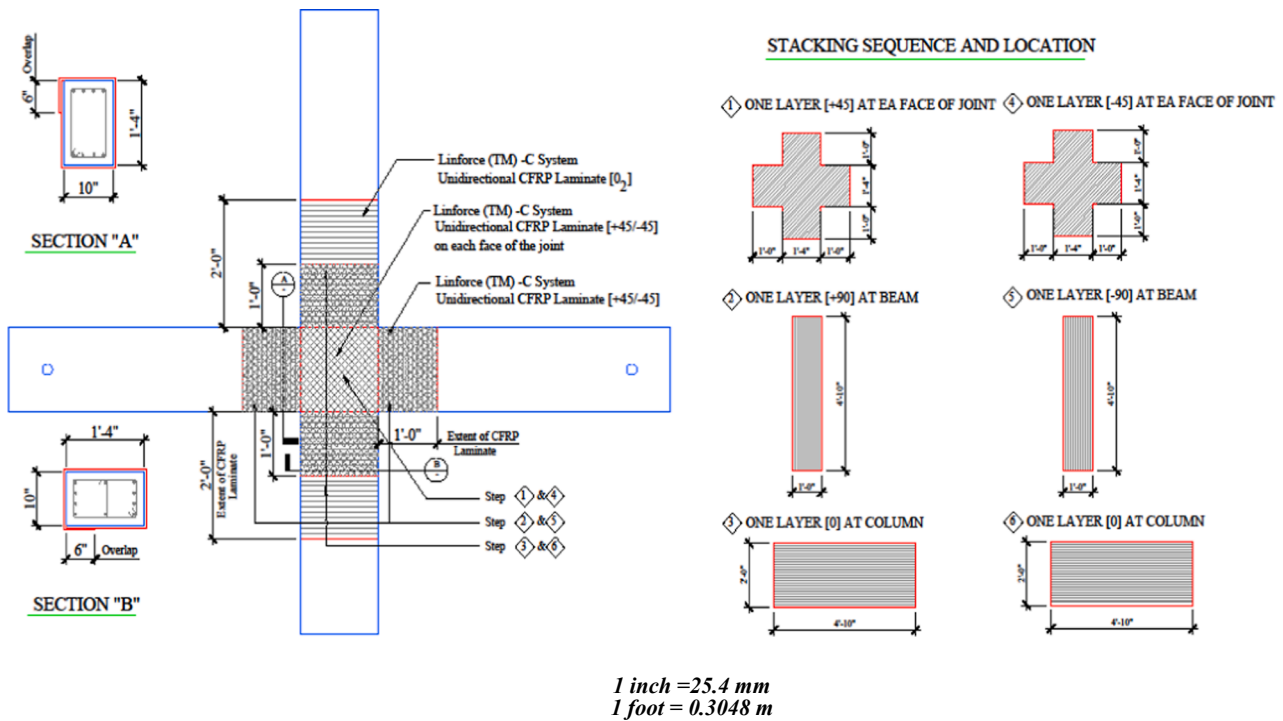
Table 3
Laminates fiber architecture and stacking sequences.

Retrofit specimen	Specimen ID	Number of plies (N_{FRP})	Laminate fiber architecture
High-strength CFRP laminates	RS-SC	8	$[0°_2/+45°/90°_2/-45°/0°_2]$ each face
GFRP laminates	RS-G	12	$[0°_3/+45°/90°_2/-45°/0°_3]$ each face
High-modulus CFRP laminates	RS-MC	4	$[0_2°/+45°/90_2°/-45°/0_2°]$ each face
High-strength CFRP laminates & composite connectors	RS-SCC	8	$[0°_2/+45°/90°_2/-45°/0°_2]$ each face

1 inch = 25.4 mm
1 foot = 0.3048 m

Fig. 13. Laminate layup sequence of repaired specimen (AR-2).

4.1. Control specimen (AB-1)

The specimen has exhibited a brittle joint shear failure. Fig. 18 shows the force-displacement backbone curve of the specimen under dynamic impulse load. The first yield in the reinforcement steel has occurred at a lateral load of 105.8 kN (23.8 kips) in the beam bottom rebar. The ultimate load was recorded at 112.0 kN (25.2 kips) corresponding to 101.6 mm (4.0 in.) lateral displacement at the top of the column. At the end of test, severe diagonal cracks were observed at the joint region. The diagonal cracks at the joint region have extended to the beam span. Severe cracks occurred at the joint corners due to excessive joint rotation. This is attributed to the absence of horizontal confinement inside the joint region needed to resist joint shear deformation. Fig. 19 shows the local damage at the joint region ultimate load.

4.2. Control specimen (AB-2)

The specimen behaved linearly in the first 71.17 kN (16.0 kips) until the first yield of reinforcement rebar occurred. The displacement-load hysteresis curve is presented in Fig. 20. In the next loading level, the rate of load increase was less than the previous cycles until the specimen reached a peak load of 99.2 kN (22.3 kips). In the following loading level, the hysteresis behavior of the specimen shows pinching, stiffness degradation and strength deterioration up to the end of the test. The peak-to-peak load variation between the push and pull cycle was small indicating the accuracy of the test setup and load application. The first hairline crack initiated at 17.8 kN (4.0 kips) in the push and pull cycle. The first yield of the reinforcement steel was monitored at 71.2 kN (16 kips) (pull cycle) in beam bottom reinforcement (BB1) rebar. The maximum push and pull load happened at the first cycle of displacement ductility level (μ_d) equal to 1.5. The maximum horizontal force was 99.2 kN (22.3 kips) in the push direction and 97.8 kN (22.0 kips) in the pull direction. During the second push cycle, strength degradation was observed. A crackling sound and crushing of the joint concrete were monitored in the second pull cycle. At displacement ductility (μ_d) equal to 2.0, a severe joint crushing was observed during

the push and pull cycles. The maximum recorded load was 53.4 kN (12.0 kips) in the push direction and 45.6 kN (10.7 kips) in the pull direction, showing significant loss in the specimen shear strength. The test was terminated at the third cycle of this displacement ductility level. The crack pattern and ultimate joint failure is presented in Fig. 21. The peak value of the normalized horizontal joint shear stress (τ_{jh}) throughout the test was equal to 14 corresponding to strain of 0.0125 in the push cycle and 17 corresponding to strain of 0.014 in the pull cycle. The specimen has dissipated a total energy equal to 25,990 kN-mm (230.0 k-in) at the end of the test. As a conclusion, the specimen exhibited a brittle mode of failure, severe degradation of strength and inadequate ductility at the joint. The experimental results show that the joint suffered severe damage and lack of ductility due to poor detailing of internal horizontal confinement inside the joint region.

4.3. Control specimen (AB-3)

Load-Displacement Hysteretic Curves is shown in Fig. 22. The first hairline crack initiated at 17.8 kN (4.0 kips) during the push and pull cycle. The reinforcement first yield occurred in the beam top reinforcement (BT2) at 53.4 kN (12.0 kips) during the pull cycle that corresponds to a displacement of 45.0 mm (1.75 in.). The maximum push and pull load recorded at the first cycle of a displacement ductility level (μ_d) equal to 1.5. At this level, the maximum recorded horizontal force was 70.7 kN (15.9 kips) in the push direction, and 71.6 kN (16.1 kips) in the pull direction. Strength degradation was recorded at the second push cycle. At displacement ductility (μ_d) equal to 2.0, the maximum load was 53.4 kN (12 kips) in the push direction and 47.6 kN (10.7 kips) in the pull direction showing significant loss in shear strength. The major crack observed through the test was at the lower left bottom corner of the beam-column interface and extended vertically along the joint. The test was terminated at the third cycle of this displacement ductility level. Rebar bond slip and cracks pattern at ultimate is shown in Fig. 23. In general, this specimen exhibited a brittle failure mode resulting in a severe joint strength degradation, poor stiffness and pinched hysteresis curves (refer to Fig. 23). The behavior
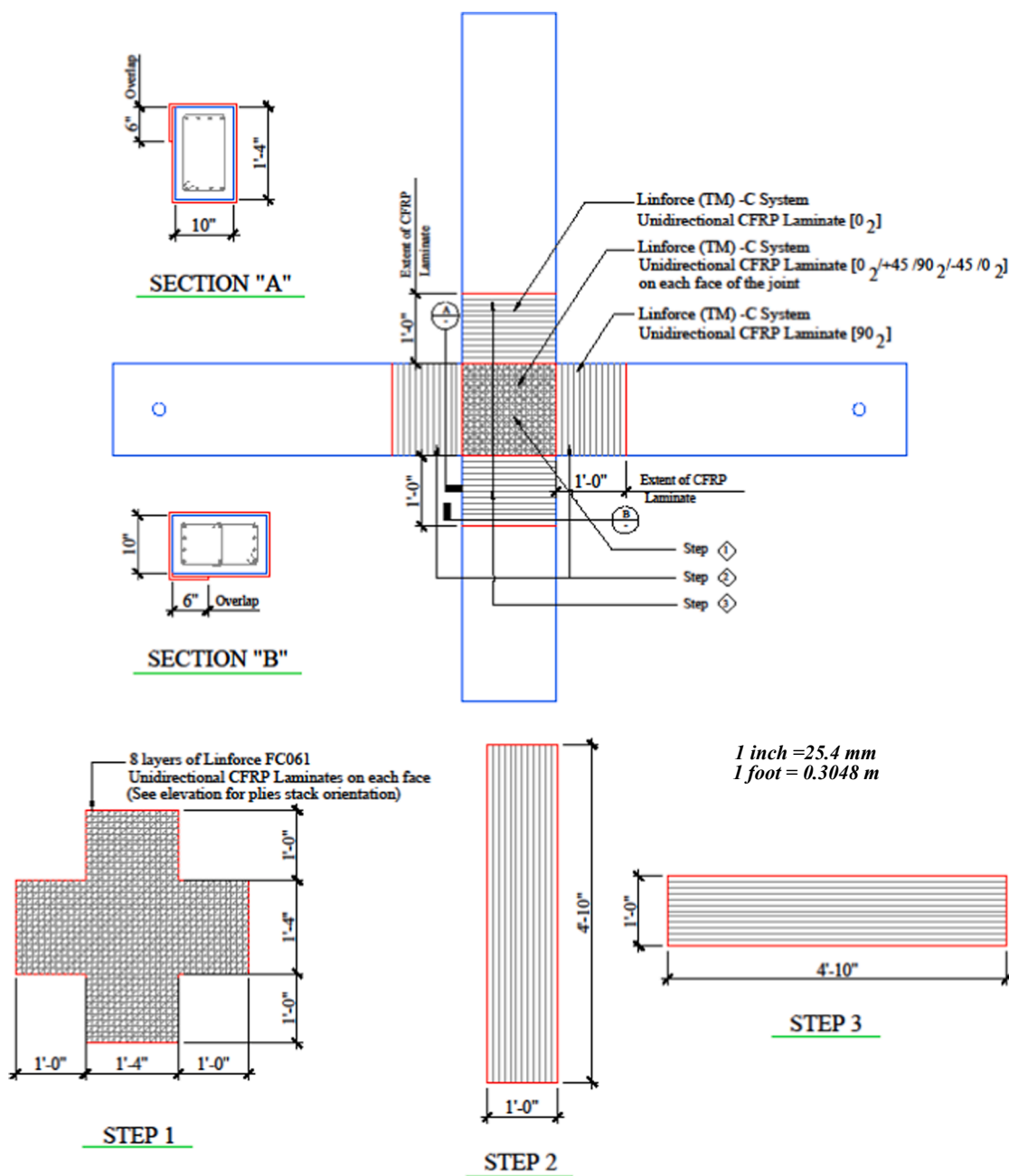
Fig. 14. Laminate layup scheme of CFRP retrofitted specimen (RS-SC).

of this specimen was dominated by diagonal joint shear cracking inside the joint region and propagation of these cracks into the beams span.

4.4. Control specimen (AB-4)

The load-displacement hysteretic curves for specimen (AB-4) are shown in Fig. 24. As shown in the figure, the load increased linear until first yielding of the reinforcement rebar occurred at a load of 80.0 kN (18.0 kips) corresponding to displacement equal to 45.0 mm (1.75 in.). After completing of the 89-kN (20-kip) cycle, the rate of gaining additional load strength reduced in the following cycle until reaching the peak load. Shear strength degradation initiated at ductility level (μd) equal to 1.5. The rate of reduction in shear strength up to failure was less than deficient control specimen (AB-2). At 75.8-mm (3-in.) displacement cycle, the peak load was recorded during the first cycle. The maximum load was 111.6 kN (25.1 kips) during the push cycle and

113.4 kN (25.5 kips) during the pull cycle. The crack width at the joint was equal to 2.5 mm (0.08 in.). During the second cycle, strength degradation was observed and concrete cover spalling at the joint zone was observed. Fig. 25 shows the ultimate failure for this joint specimen. This specimen exhibited somehow a ductile mode of failure since the strength degradation was not as severe as it was witnessed for the deficient joint described earlier. The shear strength of this joint, as compared to the deficient control specimen (AB-2), has increased only by about 14%.

4.5. Control specimen (AR-2)

The repaired specimen exhibited a brittle mode of failure, severe degradation of strength and inadequate ductility at the joint. A cracking sound was heard at the displacement of 51.0 mm (2.0 in.) at the push cycle. The maximum load at ductility level, μd, of 1.5 was 56.0 kN
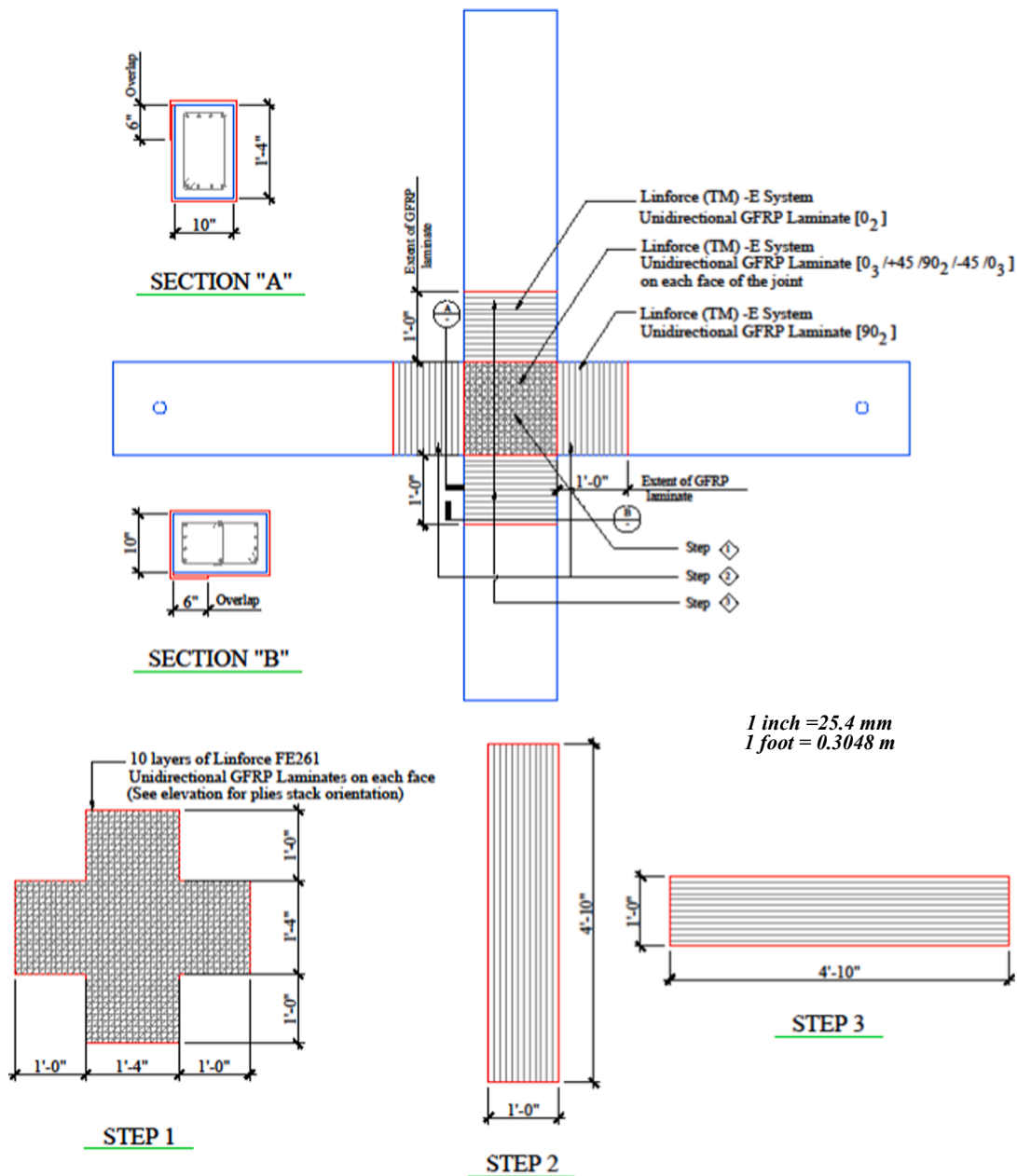
Fig. 15. Laminate layup scheme and sequence (RS-G).

(12.6 kips) at the push-cycle and 60.0 kN (13.5 kips) at the pull-cycle. These loads represent about 60% of the ultimate load strength of the control specimen. Envelopes of the load-displacement hysteresis curves are presented in Fig. 26. Debonding of CFRP laminates from the concrete surface was observed at the bottom left corner of joint. At displacement ductility of 2.0, the strength of specimen started degrading and CFRP laminates ruptured. The specimen lost its stiffness at the subsequent ductility level of 3.0. The test was terminated at the second cycle of this ductility level. Fig. 27 shows the delamination of the CFRP laminate at end of the test.

4.6. Retrofitted specimen (RS-SC)

The load-displacement hysteresis curves for this joint specimen are shown in Fig. 28. A linear load-displacement behavior was recorded up to a load equal to 80.0 kN (18.0 kips). The first yield in the reinforcement rebar was recorded in the rebar BB-6 (push cycle) at 80.0 kN (18.0 kips) corresponding to column tip displacement of 36 mm

(1.4 in.). The measured shear crack width developed at the beam side was about 0.5 mm (0.02 in.). At a displacement ductility level (μ_d) equals to 1.0, the specimen's shear strength gradually increased up to a load of 21.7 kips (96.5 kN) in the push cycle, and 114.7 kN (25.8 kips) in the pull cycle. At a displacement ductility level (μ_d) of 1.5, spalling of the concrete cover, at the column bottom, was initiated during the first cycle. The concrete spalling resulted from the induced moment caused by the cyclic horizontal load. This ductility level occurred at a load of 124.5 kN (28.0 kips) at the push cycle and about 137.8 kN (31.0 kips) in the pull cycle. In the following cycles, delaminating and de-bonding of the FRP laminates were initiated at the corners of the beam-column joint. At a displacement ductility level (μ_d) of 2.0, excessive de-bonding was observed along the joint face. In general, the strength degradation in the pull cycle was relatively larger than those observed in the push cycle. During the second push cycle of displacement ductility level (μ_d) of 2.0, FRP laminates rapture was initiated. A dramatic degradation in the load was observed in the subsequent cycles. The width of the vertical crack at the left beam was about 2.5 mm (0.08 in.). Despite the
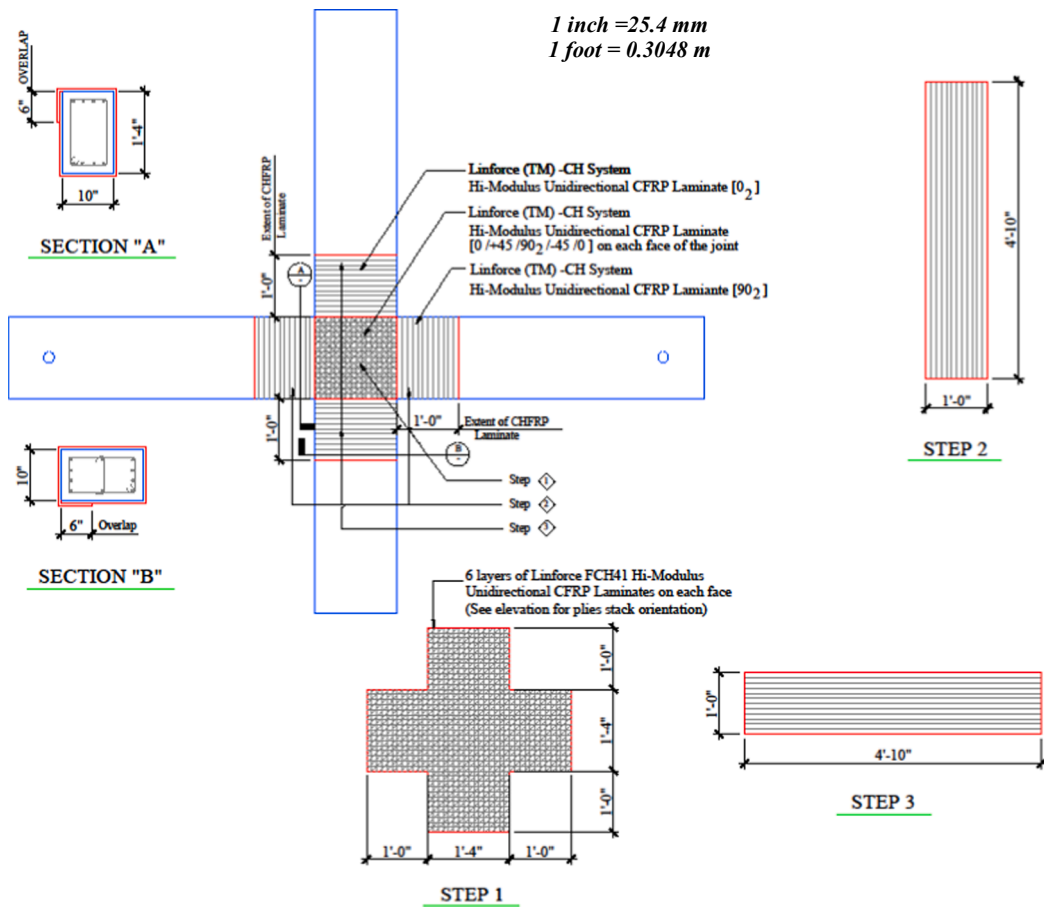
1 inch =25.4 mm
1 foot = 0.3048 m

SECTION "A"

SECTION "B"

Extent of CHFRP Laminate

Linforce (TM) -CH System
Hi-Modulus Unidirectional CFRP Laminate [0_2]

Linforce (TM) -CH System
Hi-Modulus Unidirectional CFRP Laminate
[0 /+45 /90_2 /-45 /0] on each face of the joint

Linforce (TM) -CH System
Hi-Modulus Unidirectional CFRP Lamiante [90_2]

Extent of CHFRP Laminate

Step ①
Step ②
Step ③

STEP 2

6 layers of Linforce FCH41 Hi-Modulus
Unidirectional CFRP Laminates on each face
(See elevation for plies stack orientation)

STEP 3

STEP 1

Fig. 16. Laminate layup stack for high-modulus CFRP specimen (RS-MC).

SECTION "A"

SECTION "B"

Extent of CFRP Laminate (Typ.)

10" x 10" x 10" long Advanced Pre-cured
Composite Connector w/ 2- 5/8 dia threaded
rod horiz. and vert. (Typ @ top of beam)

Linforce (TM) -C System
Unidirectional CFRP laminate [0_2]

Linforce (TM) -C System
Unidirectional CFRP laminate [0_2/+45/90_2/-45/0_2]
on each face of the joint

Linforce (TM) -C System
Unidirectional CFRP laminate [90_2]

10" x 10" x 10" long Advanced Pre-cured
Composite Connector w/ 4- 5/8 dia threaded
rod horiz. and 2-5/8 dia threaded rod vert.
(Typ @ bottom of beam)

1 inch =25.4 mm
1 foot = 0.3048 m

ELEVATION

SIDE VIEW

Fig. 17. Retrofitted specimen (RS-SCC) with CFRP laminates and hybrid composite connectors.
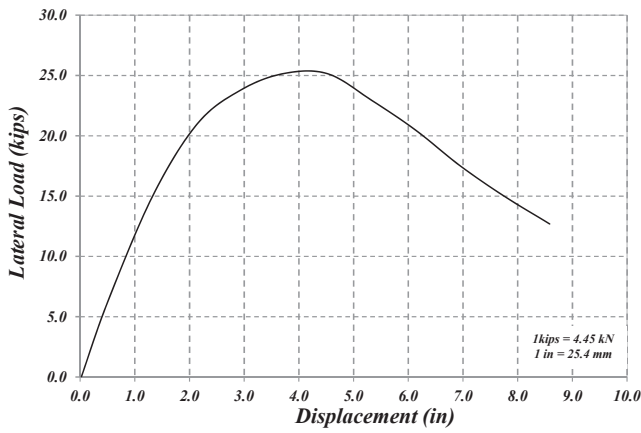
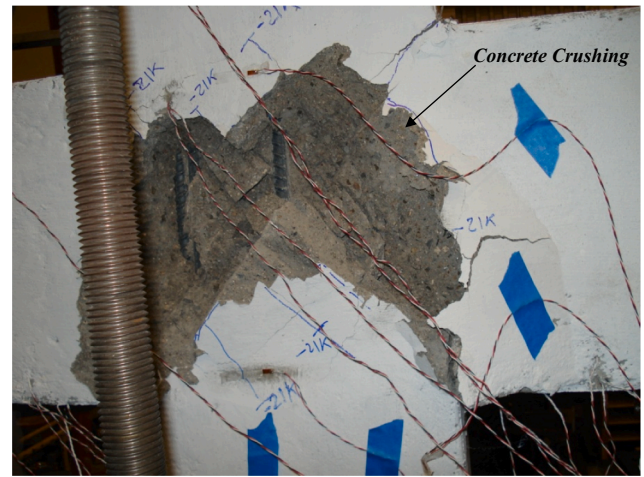**Fig. 18.** Specimen (AB-1) load-displacement curve under dynamic impulse load.

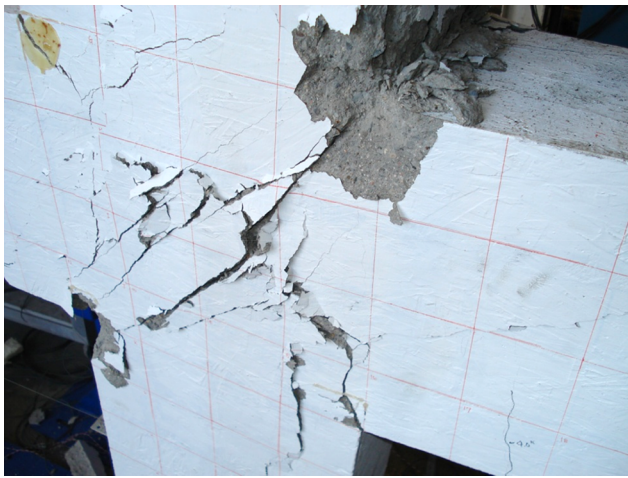**Fig. 21.** Cracks pattern at ultimate load (AB-2).

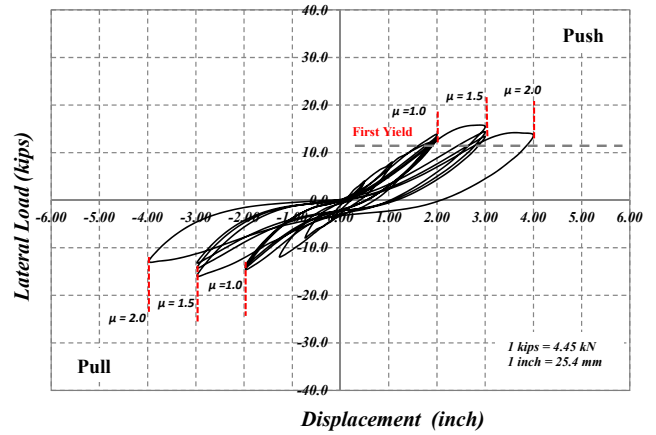**Fig. 19.** Specimen (AB-1) front view of the joint at ultimate load.

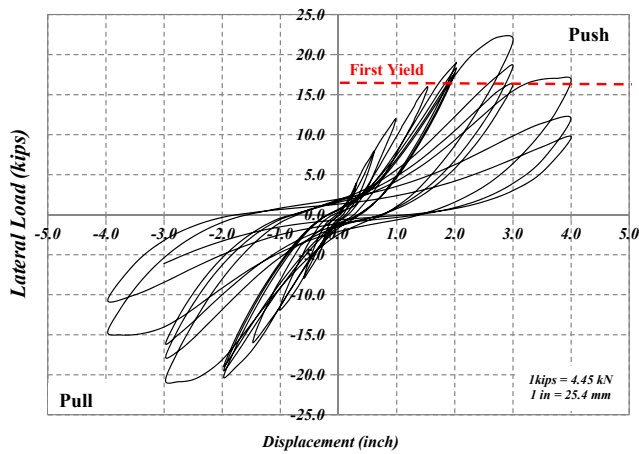**Fig. 22.** Load-displacement hysteretic curves for control specimen (AB-3).

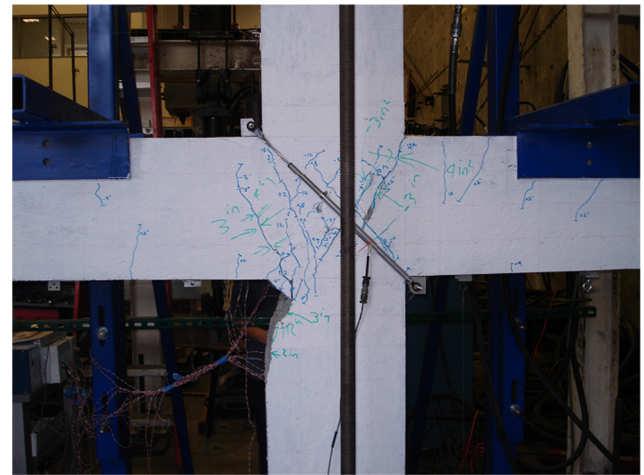**Fig. 20.** Load-displacement hysteresis curves for control specimen (AB-2).

Fig. 23. Cracks pattern at ultimate load (AB-3).

occurrence of local failure and subsequent strength degradation, test was continued and was terminated after completing an additional cycle of ductility level (μ_d) of 3.0. The CFRP laminate thin shell buckled locally at the joint region, simultaneously with crushing of the concrete cover at the joint location. A severe crushing was also observed at the base of the lower column. This can be attributed to the stress concentration that is caused by large joint rotation. The peak joint shear stress factor was 12 at a strain equal to 0.00032 in the push direction

and 16 at a strain equal to 0.00042 in the pull direction. Experimental results showed that the use of high-strength CFRP as a strengthening system, significantly improved the poor performance that was witnessed for the control joint specimen in addition to a reduction in damage initiation. The shear strength of the retrofitted joint has increased by about 36% over the identical control (strengthened) specimen (AB-2) described earlier. Fig. 29 shows the ultimate failure mode of this joint specimen.
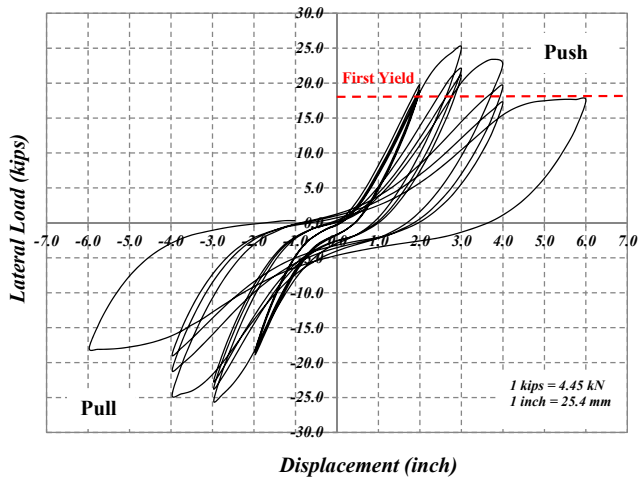
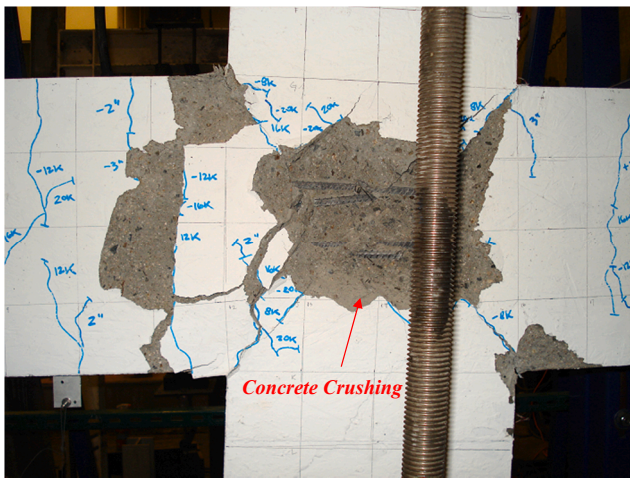**Fig. 24.** Load-displacement hysteresis curves for control specimen (AB-4).

Fig. 25. Cracks pattern of joint front face at ultimate load (AB-4).

4.7. Retrofitted specimen (RS-G)

The specimen exhibited higher ductility and strength than the control specimen. As shown in Fig. 30, a pinched hysteretic curve was observed during the linear range up to a load of 89.0 kN (20.0 kips). Following this load level, the hysteresis loops expanded indicating an increase in plastic deformation to the peak load of 111.2 kN (25.0 kips) in the push cycle and 133.5 kN (30.0 kips) in the pull cycle. During the 88.9 kN (20-kip) cycle, the first yield was observed at a load equal to 84.5 kN (19.0 kips) that corresponds to a lateral displacement of 45.0 mm (1.75 in.). Upon the completion of this cycle, the load-control protocol was switched to a displacement-control loading protocol. The maximum load achieved by this specimen occurred at the 76.0 mm (3.0 in.) displacement level. This maximum load was equal to 110.0 kN (24.7 kips) in the push direction and 131.7 kN (29.6 kips) in the pull direction. During the first cycle of the next displacement ductility level ($\mu_d = 4$), severe concrete crushing was observed at the bottom of the column as shown in Fig. 31. At this event, strength degradation was observed that can be attributed to the slippage of the lower column base at the hinged support. It is believed that the main reason for this strength degradation was due to the fact that the retrofitted joint was relatively stiff and majority of the shear forces were transferred to the base support.

4.8. Retrofitted specimen (RS-MC)

The load-displacement hysteresis curves are presented in Fig. 32. Few hair cracks initiated in the beam at 17.8 kN (4.0 kips) during the push and pull cycles. The number of cracks increased in the subsequent load levels of 35.6 kN (8.0 kips), 53.4 kN (12.0 kips) and 71.2 kN (16.0 kips). The first yield in the steel reinforcement was recorded at 86.7 kN (19.5 kips) during the push cycle at beam bottom steel rebar (BB4) at a displacement of 40.6 mm (1.6 in.). Based on the recorded first yield, idealized yield was calculated to be 52.0 mm (2.1 in.) and load-control protocol was switched to a displacement-control protocol. At a ductility level (μ_d) of 1.0, a rupture in the CFRP laminate was initiated at the joint regions during the push cycle. The maximum horizontal force recorded was 102.3 kN (23.0 kips) during the push cycle and 109.4 kN (24.6 kips) during the pull cycle. A complete rupture of the CFRP composite laminates occurred at the subsequent cycles. At the ductility level (μ_d) of 1.5, laminate rupture led to concrete
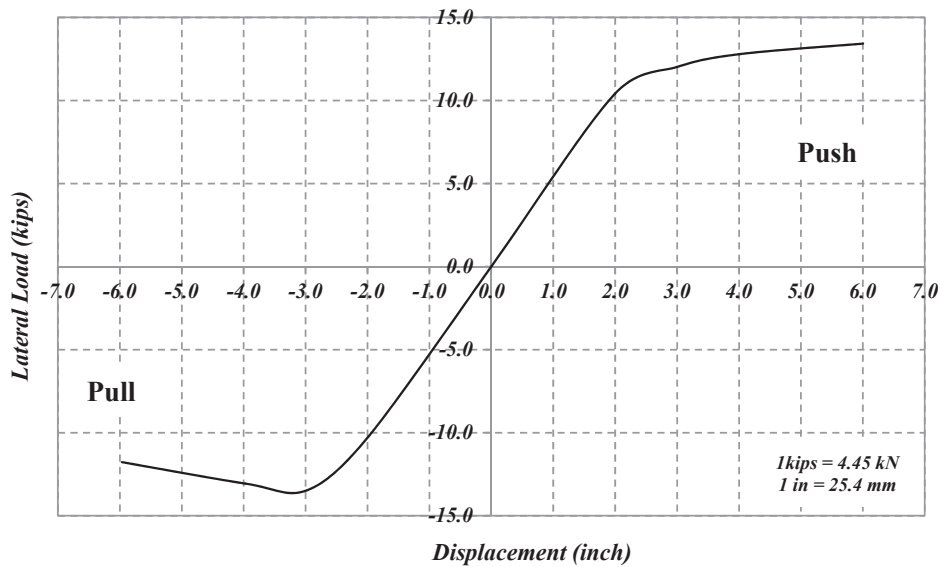

Fig. 26. Load-displacement envelope curve for repaired specimen (AR-2).
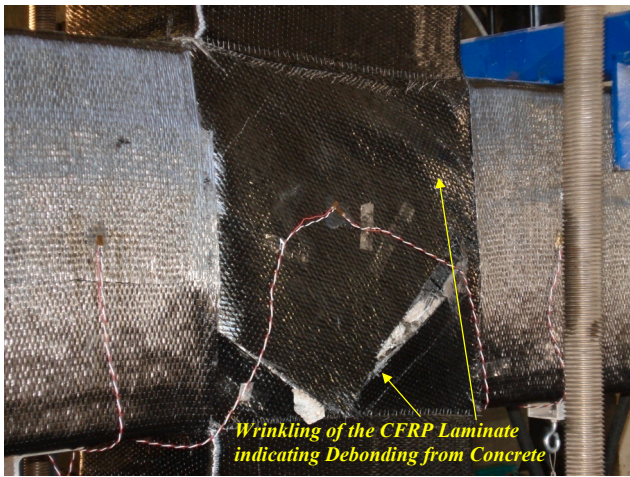
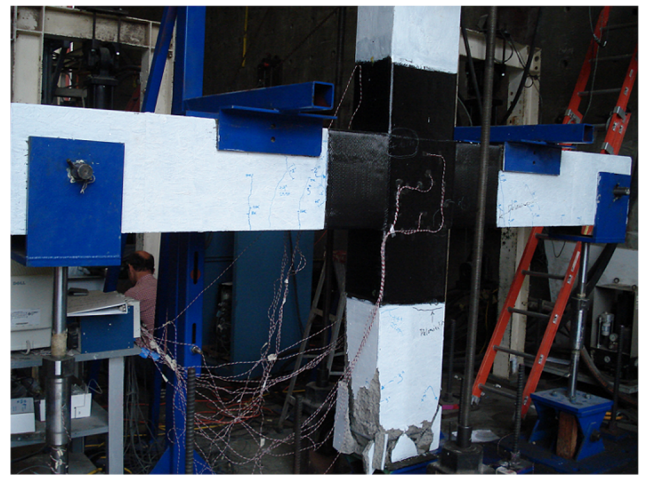**Fig. 27.** CFRP composite delamination at ultimate load (AR-2).

Fig. 29. Retrofitted specimen at ultimate load (RS-SC).

crushing that was witnessed inside the joint region coupled with strength degradation in the pull direction. The maximum pull force recorded was 97.8 kN (22.0 kips). Some residual strength monitored in the push direction and the maximum push force recorded was 107.6 kN (24.2 kips). The test was terminated after the first cycle of the next ductility level (μ_d) of 2.0. The specimen exhibited a semi-ductile failure, and higher strength as compared to the control specimen. Fig. 33 shows the rupture of the CFRP laminate at the end of the test.

4.9. Retrofitted specimen (RS-SCC)

The load-displacement and load/drift ratios hysteretic curves are presented in Fig. 34. As shown in this figure, the hysteresis curves behavior is symmetric about the horizontal axis, and the peak loads recorded pattern during both the push and pull cycles were almost identical. During early stages of loading, 17.8-kN (4-kip) cycle, hairline cracks were initiated. These cracks were continued to develop during the following cycles of 35.6-kN (8-kip) and 8.9-kN (12-kip) cycle along
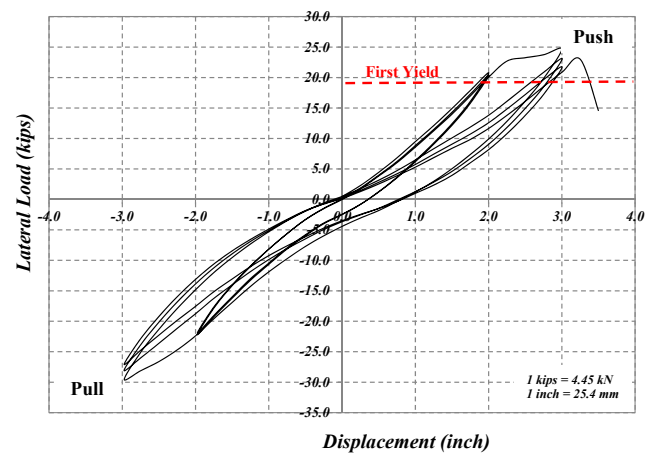

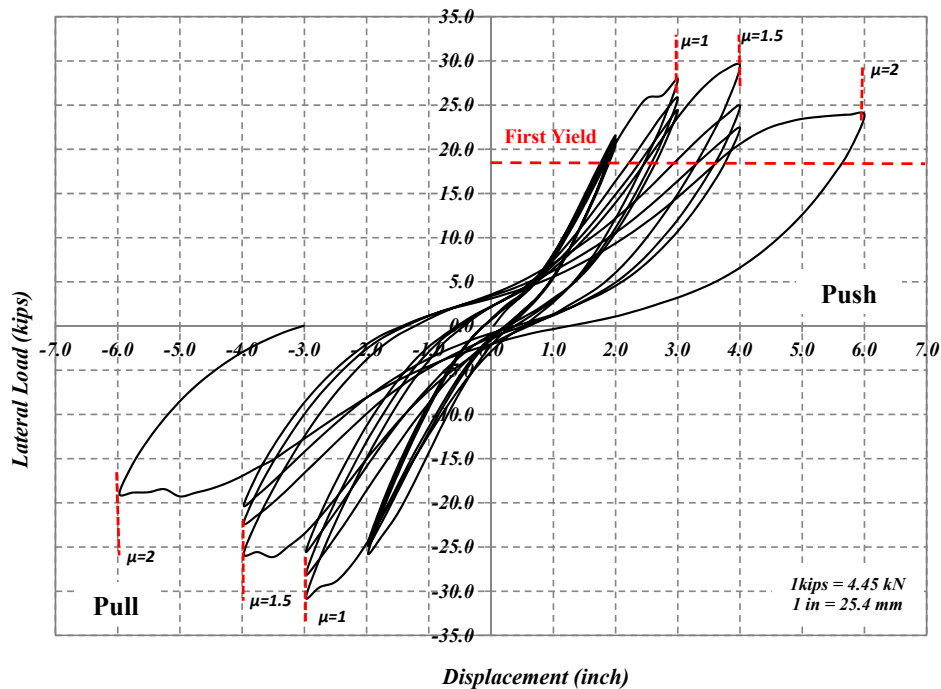**Fig. 30.** Load-displacement hysteresis curve for retrofitted specimen (RS-G).

Fig. 28. Load-displacement hysteresis curve for retrofitted specimen (RS-SC).
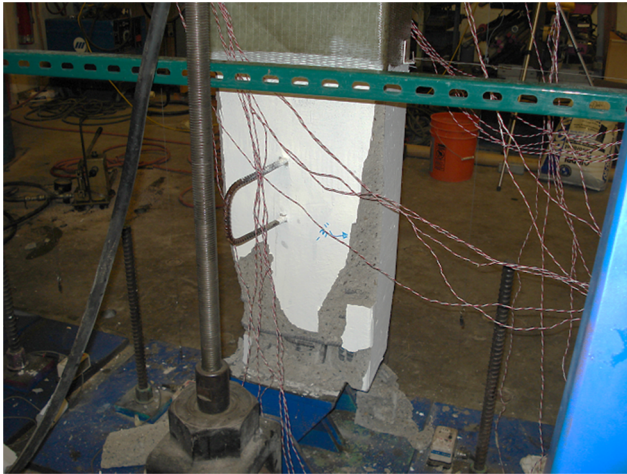
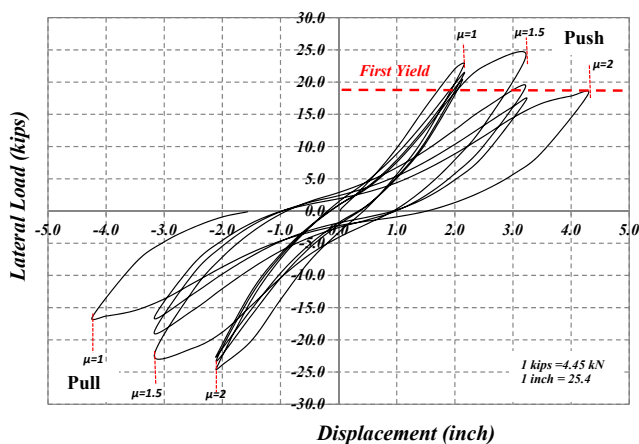**Fig. 31.** Concrete spalling at the bottom of the column at ultimate load (RS-G).

Fig. 32. Load-displacement hysteresis curve for retrofitted specimen (RS-MC).
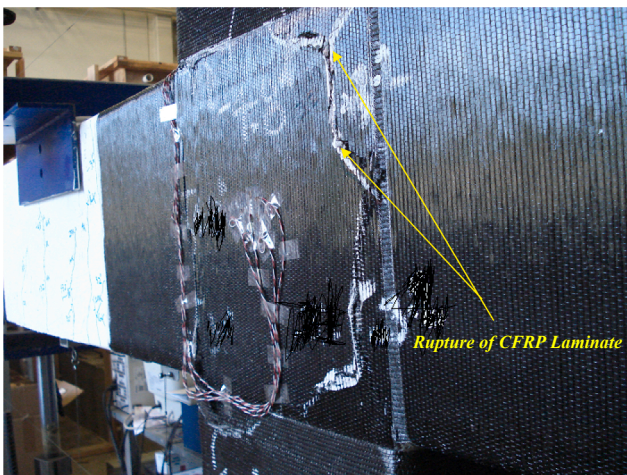

Fig. 33. Rupture of FRP at ultimate load (RS-MC).

the beam front and back sides. At these loading levels, these cracks propagated, both vertically and diagonally, during the push and pull cycles. The first yield occurred before reaching the 88.9-kN peak of (20-kip) loading cycle. At this loading level, the first yield occurred in one of the beam's longitudinal steel rebars at a load of 80.0 kN (18.0 kips) that corresponds to a displacement of 45.0 mm (1.75 in.). The beam cracks described earlier at the edge of the FRP laminate propagated through the bottom face of the beam. These cracks were the initial signs

of the formation of beam hinging mechanism. After completing the 88.9-kN (20-kip) loading cycle, the force-control protocol was ended and an idealized yield displacement of 50.4 mm (2.0 in.) was calculated. At the first displacement-control cycle of 50.4 mm (2.0 in.), the average crack width was about 3.0 mm (0.12 in.) that was propagating along the side and bottom face of the beam. At the 75.8-mm (3-in.) displacement cycle, the average crack width was about 5.0 mm (0.2 in.). At 101.6-mm (4-in.) loading cycle, excessive cracks opening were observed during the push and pull cycles. At this cycle, debonding of FRP from the concrete surface occurred along the beam depth. The recorded peak load during this loading cycle was 144.6 kN (32.5 kips) in the push cycle and 151.2 kN (34 kips) in the pull cycle. The final displacement-control cycle was 152.2 mm (6 in.). At this final loading cycle, load was slightly increased to 151.2 kN (34 kips) during the push cycle, however, no increase in the joint's shear strength in the pull cycle was observed. After completing the first cycle of this displacement level, excessive strength degradation was observed. The specimen completed a full cycle at the 152.4 mm (6 in.) displacement loading level in both of the push and pull direction before any strength degradation. At a drift ratio of 5.0%, a shear strength degradation of 29%, in the second cycle, occurred as compared to the peak load recorded in the first cycle. At this point, a plastic hinging mechanism in the beam was observed. The test was ended by completing the second cycle of this load level. Fig. 35 shows cracks distribution and debonding of the CFRP laminates at the beam edge side of this specimen. Based on the observed cracks, this specimen exhibited a ductile behavior as compared to the brittle joint shear failure that was witnessed for the control (as-built) specimen. The ultimate governing failure mode was in the form of the development of a plastic hinge at the beam section. This hinging mechanism was relocated away from the joint region and moved to the beam end span (strong column/weak beam desirable failure pattern). The amount of energy dissipated at the first eight cycles was about 10% that was dissipated at the end of the test. This was observed through the initiation of minor hair cracks at the connector edge. After this stage, a steady-state pattern up to fourteenth cycle was observed. This may be attributed to the initiation of the plastic hinging mechanism at the beam span. The specimen stiffness has degraded by 79% from the corresponding stiffness measured during the first to last displacement-control loading cycle. The retrofitted specimen has achieved a significant improvement in promoting ductile behavior by formation of beam hinging mechanism. The use of the hybrid composite connectors delayed the brittle joint shear failure and the beam's bottom steel reinforcement pullout. The overall performance of the specimen shows a ductile behavior with a peak shear strength 2.5 times the story shear resisted by the control (as-built) specimen.

5. Comparison between behavior of different FRP retrofit schemes

The following sections discuss the difference in behavior of different FRP retrofitting schemes evaluated and developed in this study. Five comparison categories are discussed including: (i) modes of failure, (ii) load-displacement envelopes, (iii) energy dissipation capacity, (iv) stiffness degradation, and (v) joint ductility.

5.1. Modes of failure

In order to evaluate seismic performance improvement of a retrofitted specimen, the mode of failure of both the deficient (as-built) and retrofitted specimen were identified based on the observation of the large-scale experimental test results. The mode of failure and ductility are the main indicators for measuring the enhancement of existing deficient joint when retrofitted with the proposed retrofitting system. As for the control (as-built) specimen with shear deficiency, the observed failure was in the form of rapid development of diagonal shear cracks that were initiated along both faces of the beam-column joint. These cracks propagated throughout the test and ended with concrete
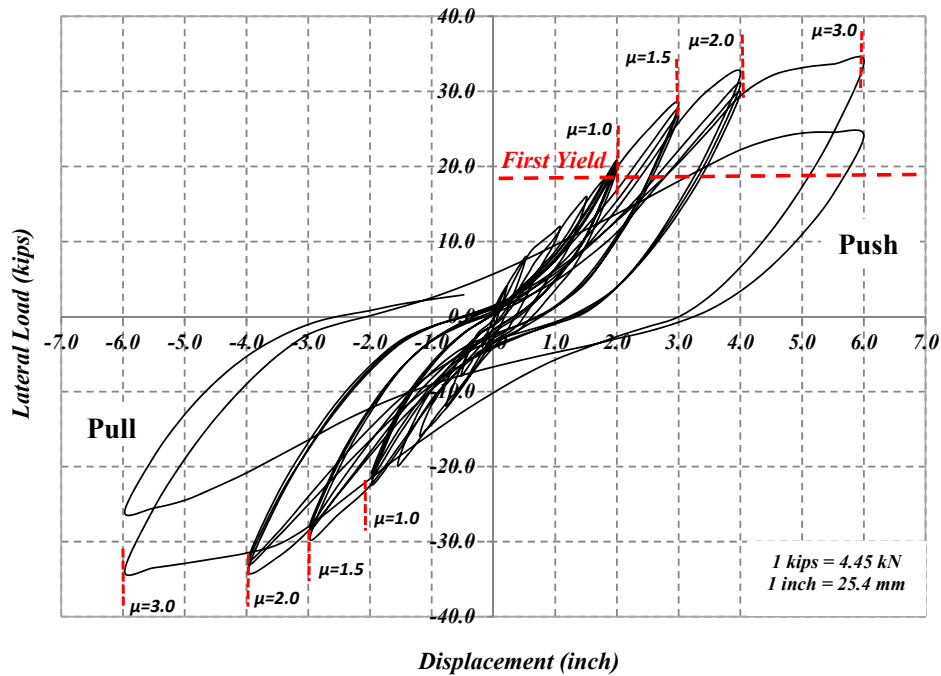
Fig. 34. Load-displacement hysteresis curves for retrofitted specimen (RS-SCC).
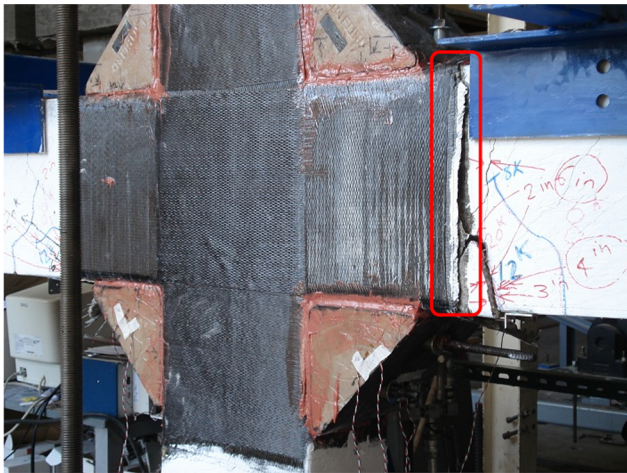

Fig. 35. FRP debonding at ultimate load.

crushing of the joint core. The dominating mode was in the form of a brittle joint shear failure. Similar behavior was observed for the control specimen with both shear and rebars bond-slip deficiencies. However, excessive cracks and crushing of the bottom face of one of the beams was observed due to bond-slippage of discontinuous beam rebars. The failure mode of the last control beam-column joint specimen designed per the current ACI318-14 code [3] was dominated by a semi-ductile mode of failure. This specimen showed some ductile behavior through energy dissipation, however, ultimately concrete crushing of the joint region occurred due to over the relatively lower strength of the beam section required by the current ACI code in order to maintain the weak beam-strong column protocol.

Regardless of the retrofitted system used for enhancing joint shear deficiency, the denominated mode of failure for all the retrofitted specimens was the rupture of the FRP composite laminate except for the retrofitted specimen with E-glass/epoxy composite system. The failure of retrofitted specimen with high-strength CFRP composite laminates was dominated by debonding of the FRP laminates at the corners of the

joints. The debonding of the FRP laminates propagated throughout the test leading to dilation of the unconfined concrete core inside the joint. Once the composite plies reached their ultimate strain, the FRP laminates ruptured and the specimen failed due to excessive lateral deformation. Similar behavior was observed for the retrofitted specimen with high-modulus epoxy CFRP system except that the specimen failed at a lower shear strength due to the laminate relatively limited rupture strain. In case of E-glass/epoxy retrofitted specimen, the specimen failed due to crushing of the concrete at the base of the lower column end. This specimen failed prematurely due to excessive shear load at the column base. The last specimen retrofitted with high-strength CFRP laminates and hybrid composite connectors that was designed for improving joint shear strength and rebars bond-slip performance failed in a ductile mode. This retrofitting system was capable of relocating the plastic hinge away from the joint region and shifted the hinge location to occur at the edge of composite connectors. In addition, this specimen dissipated a significant amount of energy through the use of the innovative retrofitted system. The system was capable of maintaining the integrity of the joint with forcing the desirable ductile behavior to occur in the beam element satisfying the safe strong column/weak beam design protocol. Table 4 summarize different modes of failure for all control and retrofitted specimens. As shown in this table, specimen description, designated code and ultimate mode of failure for each specimen are presented.

5.2. Load-Displacement envelopes

A comparison between the load-displacement curves of both deficient and retrofitted specimens. In order to realize beam-column joint shear strength enhancement, hysteretic envelopes of load-displacement curves for the deficient specimen (AB-2), control specimen (AB-4) designed per ACI318-14 [3], and the retrofitted specimen with different FRP composite laminate are compared in Fig. 36. The improvement in joint shear strength and rebar bond slip between the deficient and retrofitted specimen (RS-SCC) using high-strength carbon/epoxy laminates and advanced composite connectors, the load-displacement hysteresis curves envelope is presented in Fig. 37.

Table 4
Comparison of modes of failure for different specimens.

Specimen's description	Specimen's designation	Mode of failure
Control (As-Built) specimens		
Control specimen with joint shear deficiency	AB-1	Brittle shear failure at the joint
Control specimen with joint shear deficiency	AB-2	Brittle shear failure at the joint
Control specimen with joint shear deficiency and beam rebar bond slip	AB-3	Brittle shear failure at the joint accompanied with pullout of beam bottom rebar
Control specimen with joint designed per ACI-318 code [3]	AB-4	Partial ductile failure at the joint
Repaired specimen		
As-built damaged specimen (AB-2) repaired with high-strength CFRP laminates	AR-2	Brittle failure mode and severe strength degradation at the joint
Retrofitted specimens		
Retrofitted joint with high-strength carbon/epoxy FRP laminates	RS-SC	Concrete crushing inside the joint region due to delaminating and debonding of CFRP laminates at the joint
Retrofitted joint with E-glass/epoxy FRP laminates	RS-G	Concrete toe crushing at the bottom of the column due to excessive base shear reaction
Retrofitted joint with high-modulus carbon/epoxy FRP laminates	RS-MC	Concrete crushing inside the joint region due to rupture of high-modulus CFRP laminates at the joint
Retrofitted joint with high-strength carbon/epoxy FRP laminates and composite connectors	RS-SCC	Plastic hinging mechanism at the beam span and relocating of the failure away from the beam-column joint

5.3. Energy dissipation capacity

The energy dissipation of the deficient control specimen was compared with the retrofitted specimens as well as the control specimen designed per the ACI318-14 code [3] requirements. A comparison between energy dissipation of deficient and retrofitted specimens is presented in Fig. 38. As shown in this figure, specimen (RS-SC), retrofitted with high-strength CFRP composite laminates, attained the highest energy dissipation capacity as compared to other specimens. This can be attributed to the relatively higher CFRP laminate rupture strain that allowed the specimen to dissipate significant amount of energy prior to reaching its ultimate failure load. The energy dissipated by specimen

(RS-SC) was about 1.7 times the control specimens (AB-2) and (RS-MC).

A bar chart comparison of energy dissipated by control specimen (AB-3) that was deficient in both shear and bond-slip, the control specimen (AB-4) designed per current ACI318-14 code [3], and the retrofitted specimen (RS-SCC) strengthened with high-strength CFRP laminates/advanced composite connectors is presented in Fig. 39. From this figure, one can see that the retrofitted joint specimen (RS-SCC) has dissipated energy about 4.5 times the control (as-built) specimen (AB-3) and 3.5 times the control specimen (AB-4). This superior performance may be attributed to the formation of the desirable plastic hinging at the beam span. The specimen has exhibited a ductile mode of failure during the different stages of loading up to its ultimate failure.
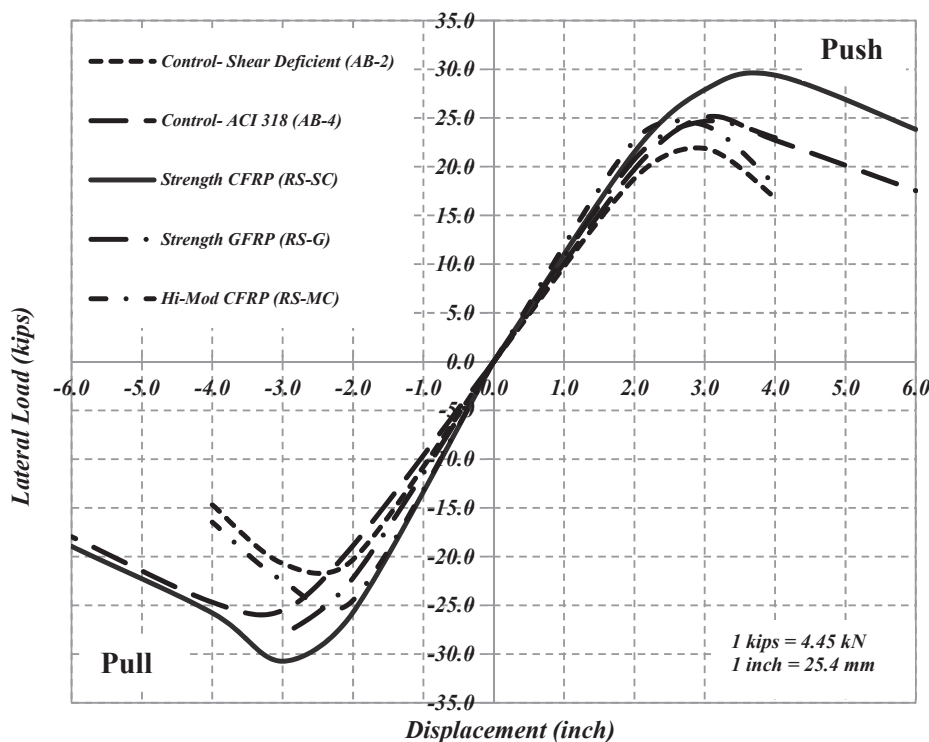

Fig. 36. Load-displacement envelope for shear deficient control and retrofitted specimens.
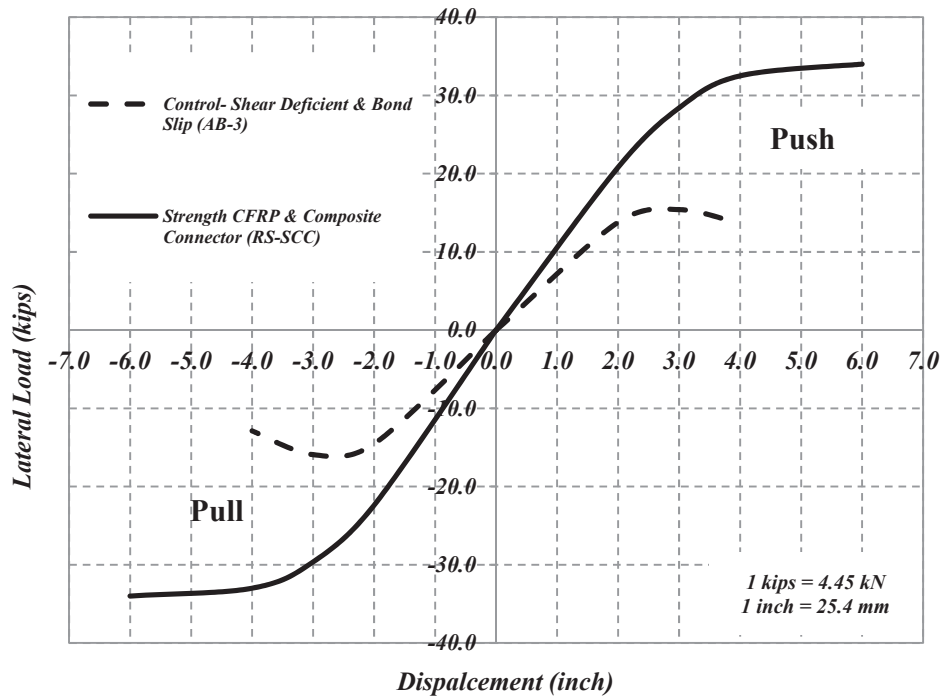
Fig. 37. Load-displacement envelope for shear & bond slip deficient control and retrofitted specimens.

5.4. Stiffness degradation

As mentioned earlier, the stiffness degradation is defined as the slope of the connecting line between the positive and negative peaks at each cycle. Fig. 40 shows a comparison between stiffness degradation of shear deficient specimen (AB-2), and retrofitted specimens (RS-SC), (RS-G) and (RS-MC). From this figure, one can notice that specimen (RS-SC) had the most even distribution in stiffness degradation among other joint specimens. Fig. 41 shows the comparison of stiffness degradation of bond-slip deficient specimen (AB-3), and specimen (RS-SCC) that with retrofitted with both high-strength CFRP composite

laminates and hybrid composite connectors. As shown in the figure, the retrofitted specimen (RS-SCC) had much better stiffness degradation distribution than the control specimen (AB-3).

5.5. Joint ductility

In order to highlight the ductility enhancement of the retrofitted joint specimens as compared to the as-built specimens, a comparison between the ductility of both groups was identified. The displacement ductility capacity is defined as the ratio of the displacement capacity to the idealized yield displacement. To calculate the ductility capacity, the
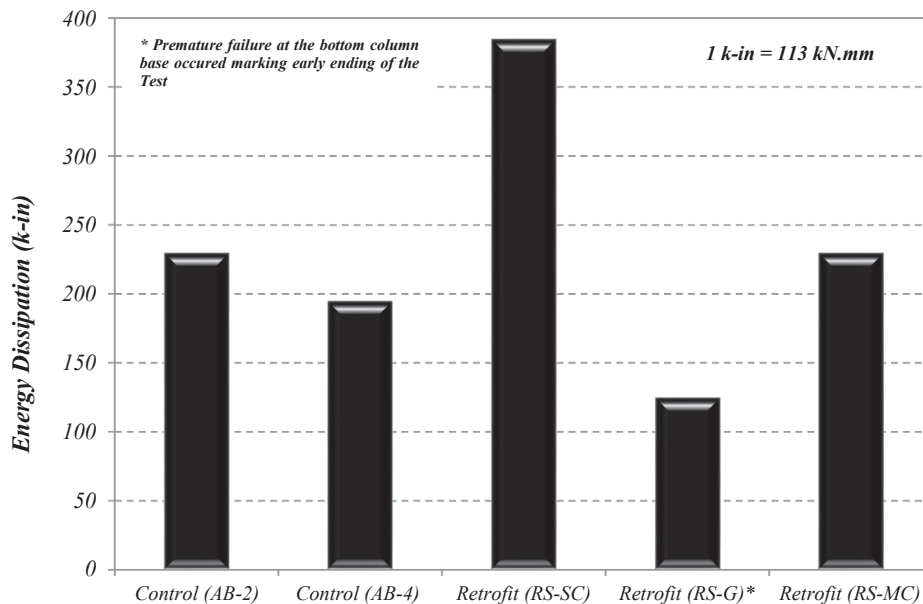

Fig. 38. Energy dissipation comparison between: (i) deficient control specimen in shear, (ii) control specimen per ACI-318 [3], and (iii) retrofitted specimens.
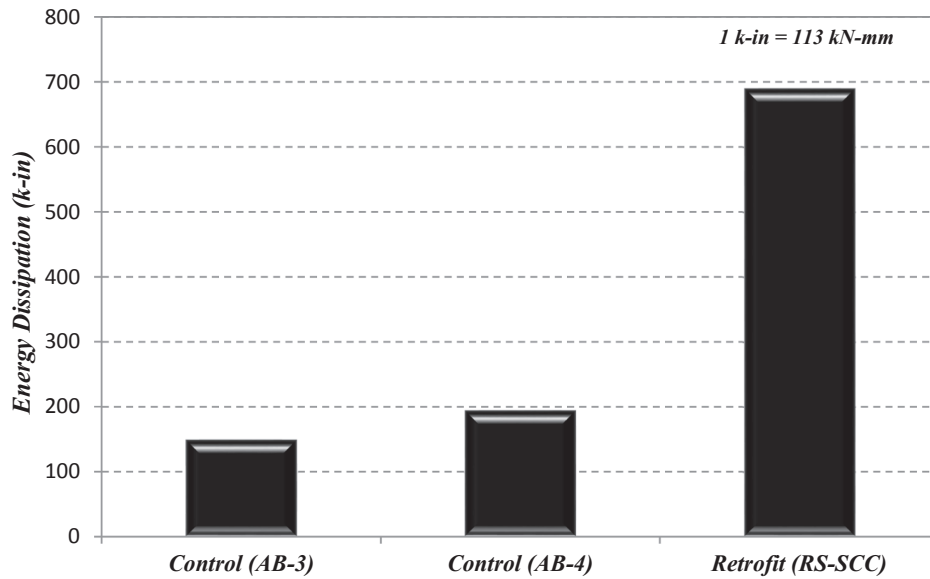
Fig. 39. Energy dissipation comparison between: (i) deficient control specimen in shear & bond slip, (ii) control specimen per ACI-318 code [3], and (iii) retrofitted specimen (RS-SCC).
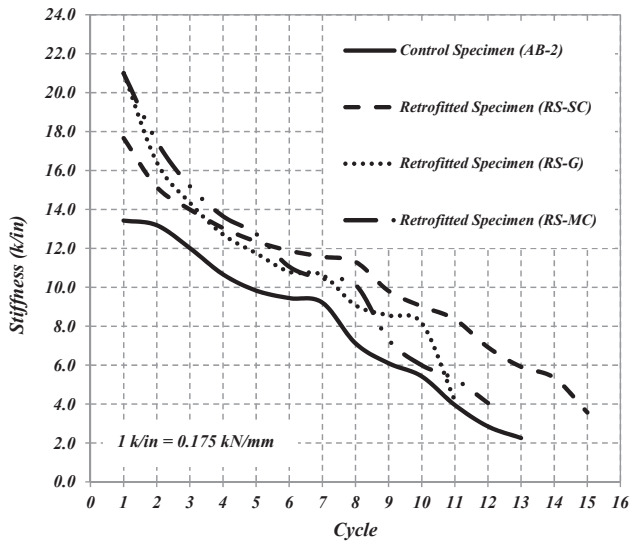

Fig. 40. Stiffness degradation comparison between: (i) deficient control specimen (AB-2), and (ii) retrofitted specimens (RS-SC), (RS-G) and (RS-MC).

Fig. 41. Stiffness degradation comparison between: (i) deficient control specimen (AB-3), and (ii) retrofitted specimen (RS-SCC).

following expression was used:

$$\mu_c^* = \frac{\Delta_c}{\Delta_y} \tag{13}$$

where Δ_c is the displacement capacity at peak and Δ_y is the idealized yield displacement. The ductility capacity comparison between different specimens is shown in Table 5.

6. Conclusions and recommendations

Experimental results indicated that FRP composite systems proposed in this study succeeded in enhancing the strength, stiffness and ductility of the seismically deficient reinforced concrete beam-column joint. The test setup was capable of capturing the shear deficiency behavior of the beam-column joint and the enhancement in its behavior after retrofit.

The proposed strengthening techniques for improving the shear strength of the beam-column joint using high-strength carbon fiber
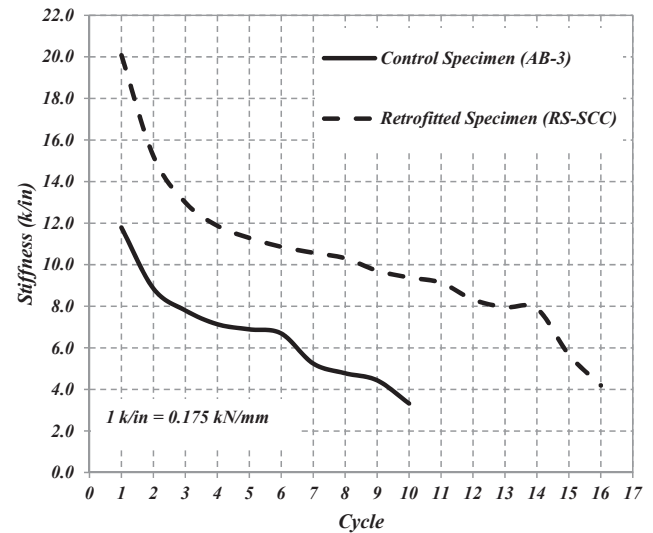
Table 5
Comparison of ductility capacity between different specimens.

	Yield displacement (Δ_y), mm (inch)	Peak displacement (Δ_c), mm (inch)	$\mu_c = \frac{\Delta_c}{\Delta_y}$	$\mu_c^* = \frac{\Delta_c}{\Delta_y}$
Control (AB-2)	38.0 (1.50)	70.0 (2.75)	1.84	1.37
Control (AB-3)	45.0 (1.75)	70.0 (2.75)	1.57	1.18
Control (AB-4)	45.0 (1.75)	77.0 (3.00)	1.72	1.28
Retrofitted (RS-SC)	36.0 (1.40)	102.0 (4.00)	2.86	2.15
Retrofitted (RS-G)	46.0 (1.75)	77.0 (3.00)	1.72	1.28[**]
Retrofitted (RS-MC)	41.0 (1.60)	83.0 (3.25)	2.03	1.53
Retrofitted (RS-SCC)	45.0 (1.75)	153.0 (6.00)	3.43	2.57

[*]Based on idealized yield displacement.
[**] Pre-mature failure at the bottom column base.

reinforced polymer composites, E-glass fiber reinforced polymer composites and high-modulus carbon fiber reinforced polymer composites were successful. Using the proposed retrofitting systems, a significant enhancement in the joint shear strength was achieved. The retrofitted specimen (RS-SC) with high-strength carbon/epoxy composite laminates improved the joint shear strength capacity by 1.34 times the control deficient specimen (AB-2).

Although the initial performance of the E-glass/epoxy retrofitted specimen was satisfactory, and due to premature localized failure at the support, complete information to assess the performance of this type of retrofitting system was not achieved in this study. This in return posed difficulties to validate the efficiency of the numerical model. Future work in this area is recommended in order to evaluate such system.

Experimental results indicated that the use of high-modulus carbon/epoxy composites for joint deficiency application was not as successful as expected. This may be attributed to two factors, including: (i) FRP composite laminates with higher stiffness at the just location attracted more stresses, causing an earlier strength degradation at these locations, and (ii) due to the high modulus of such laminates, the plastic deformation at the joint was limited resulting in a lower overall ductility of the retrofitted specimen. This was illustrated in Fig. 36 and Table 5. For example, ductility of the high-modulus/epoxy retrofitted specimen was 36% lower than as compared to the high-strength carbon/epoxy retrofitted specimen.

The proposed technique used in retrofitted specimen (RS-SCC) for enhancing the rebar bond slippage and shear strength of the joint using high-strength CFRP laminate and hybrid composite connector was also successful. This innovative technique improved the shear strength of the joint 2.5 times the control deficient specimen. The use of the hybrid composite connector prevented brittle shear failure inside the joint region and allowed a plastic hinge to develop away from the column face. The energy dissipation of the retrofitted specimen (RS-SCC) was 4.6 times the control specimen (AB-3) with discontinuous reinforcement rebars.

The innovative hybrid composite connectors developed by the second author provided an effective, yet very economical alternative for retrofit of bond-slip of deficient joint. The hybrid composite connector can easily be fabricated at the field with minimum cost. The reliability and efficiency of these connectors have been confirmed from both experimental and numerical results. It should be noted that after the ultimate failure of the retrofitted specimen (RS-SCC) that no crack or any apparent damage and no bond failure occurred at any connector or connector interface. This hybrid connector is believed to be useful for the area application including new construction and pre-cast concrete joints, as well as repair of damaged steel joint (i.e. particular in parking structures).

Based on the results of this study, the following are recommendations for future research:

1. This research focused on two weaknesses of reinforced concrete frame structures that were built using 1970s construction details as discussed by Beres et al. [12]. Hence, the other deficiencies namely beam-column moment capacity, column reinforcement ratio less than 2%, column lap splicing location, and construction joint location should be evaluated.
2. The FRP materials evaluated in this study including high-strength CFRP/epoxy, high-modulus CFRP/epoxy and E-glass/epoxy laminates. Other types of fibers such as aramid (Kevlar™), steel/composite laminates, basalt composites should be evaluated to increase the choice for structural upgrade for retrofitting existing deficient buildings.
3. Although the innovative hybrid composite connectors developed by the second author was extremely successful to retrofit rebars bond-slip, other geometries including hollow connector, connector with outside laminates made of other composites such as E-glass, S-glass, aramid may provide equal or better performance. Currently, work in

progress to optimize the performance and the geometry of such connectors.
4. Both high-strength epoxy gel and steel threaded rods were used to attach the HCC connectors to both beams and columns. It is recommended to evaluate other attachment methods including bolted only, bonded only or other innovative joining techniques.
5. One important issue that was not covered within the scope of this paper is the durability of both the composite laminates and the adhesive system that include fire exposure which is a high risk for buildings, in particular schools and hospitals. A comprehensive study on this issue is highly recommended to evaluate the effect of stiffness and strength degradation on the service performance of such techniques.
6. Due to the fact that both polymer composites and connector materials are considered to be viscoelastic materials, the issue of creep and creep rupture is very critical. For this reason, it is highly recommended to evaluate the long-term creep behavior of the retrofitted specimens under various stress levels and environmental exposures. This is essential to determine both the stiffness and strength limit states design.
7. As mentioned in the preceding conclusion section, and due to the lower ductility and strength of the beam-column specimen retrofitted with high-modulus CFRP (Specimen RS-SC), it is believed that this type of polymer composites is not suited for joint retrofit application. However, this type of CFRP composite laminates may be more applicable for column confinement, beam and floor flexural strengthening where the efficiency of the retrofit materials is proportional to the modulus of the composites due to the strain compatibility requirements.

Declaration of Competing Interest

The authors declared that there is no conflict of interest.

Appendix A. Supplementary material

Supplementary data to this article can be found online at https://doi.org/10.1016/j.engstruct.2019.109308.

References

[1] American Concrete Institute (ACI). Building code requirements for structural concrete. ACI Committee 318; 1963.
[2] American Concrete Institute (ACI). Recommendations for design of beam-column connections in monolithic reinforced concrete structures. Joint ACI-ASCE Committee 352, ACI352R-76, ACI Journal, Proceedings 1976; 73(7): 375–93.
[3] American Concrete Institute (ACI). Building code requirements for structural concrete and commentary, ACI Committee 318, ACI318-14; 2014.
[4] Mosallam A, Allam K, Salama M. Analytical and numerical modeling of RC beam-column joints retrofitted with FRP laminates and hybrid composite connectors. Compos Struct 2019;214(2019):486–503.
[5] Sengupta AK, Reddy CS, Badarinarayanan VT, Asokan A. Seismic analysis and retrofit of existing multi-storeyed buildings in India-an overview with a case study. In: 13th world conference on earthquake engineering. BC, Canada: Vancouver; 2004. Paper (No. 2571).
[6] Paulay T, Park R, Priestley MJN. RC beam column joints under seismic actions. ACI Struct J 1978;75(11):585–93.
[7] Hakuto S, Park R, Tanaka H. Seismic load tests on interior and exterior beam-column joints with substandard reinforcing details. ACI Struct J 2000;97(1):11–25.
[8] Hanson NW, Connor HW. Seismic resistance of reinforced concrete beam-column joints. J Struct Div ASCE 1967;93(5):533–60.
[9] Corazao M, Durrani AJ. Repair and strengthening of beam-to-column connections subjected to earthquake loading. NCEER technical report no 89-0013. National Centre for Earthquake Engineering Research; 1989. 93 p.
[10] Fujii F, Morita S. Comparison between interior and exterior reinforced beam-column joint behaviour. ACI-SP 123, design of beam-column joints for seismic resistance; 1991. p. 145–65.
[11] Aycardi L, Mander J, Reinhorn A. Seismic resistance of reinforced concrete frame structures designed only for gravity loads: experimental performance of sub-assemblages. ACI Struct J 1994;91(5):552–63.
[12] Beres A, Pessiki S, White R, Gergely P. Implications of experimental on the seismic behavior of gravity load designed RC beam-to-column connections. Earthquake Spectra 1996;12(2):185–98.

[13] Choudhuri D, Mander J, Reinhorn A. Evaluation of seismic retrofit of reinforced concrete frame structures: Part I-Experimental performance of retrofitted sub-assemblages. Technical Report NCEER-920030, Buffalo; 1992.

[14] Bracci J, Reinhorn A, Mander J. Seismic resistance of reinforced concrete frame structures designed for gravity loads: performance of structural system. ACI Struct J 1995;92(5):597–609.

[15] Cosenza E, Manfredi G. Some remarks on the evaluation and strengthening of underdesigned R.C. frame buildings. NCEER technical report no 97-0003, 185-175; 1997.

[16] Kurose Y, Guimaraes G, Liu Z, Kreger M, Jirsa JO. Study of reinforced concrete beam-column joints under uniaxial and biaxial loading. PMFSEL report no 88-2. University of Texas at Austin; 1998.

[17] Walker SG. Seismic performance of existing RC beam-column joints. University of Washington; 2001. MSCE thesis.

[18] Prison HGL, Baraka M. Grouted steel tubes as seismic retrofit for beam to column joints. In: Proceedings, 7th Canadian conference on earthquake engineering, Montreal; 1995. p. 871–8.

[19] Appa Roa G, Mahajan M, Gangaram M. Performance of nonseismically designed RC beam-column joints strengthen by various schemes subjected to seismic loads. J Struct Eng 2008;35:52–8.

[20] Biddah A, Ghobarah A, Aziz TS. Upgrading of nonductile reinforced concrete frame connections. J Struct Eng 1997;123(8):1001–10.

[21] Mosallam AS. Strength and ductility of reinforced concrete moment frame connections strengthened with quasi-isotropic laminates. Compos B Eng 2000;31(6–7):481–97.

[22] Mosallam AS. Chapter on composites in construction. Chapter 45, Materials selection handbook. NY, USA: John Wiley Publishing Co.; 2002. 53 ps.

[23] Mosallam AS, Bayraktar A, Elmikawi M, Pul S, Adanur S. Polymer composites in construction: an overview, SOJ Materials Science & Engineering, Symbiosis, Open Access; 2015. p. 1–25.

[24] Mukherjee A, Joshi M. FRPC reinforced concrete beam-column joints under cyclic excitation. J Compos Struct 2004;70:185–99.

[25] Antonopoulos C, Triantafillou TC. Experimental investigation of FRP strengthened RC beam-column joints. J Compos Constr 2003;7(1):39–49.

[26] Ayala D, Penford A, Valentini S. Use of FRP fabric for strengthening of reinforced concrete beam-column joints. In: Proceedings of structural faults + repair. The Commonwealth Institute, London, CD-ROM; 2003.

[27] Mahini SS, Ronagh HR. CFRP-retrofitted RC exterior beam-column connections under cyclic loads. FRP Compos Civil Eng 2004;31:647–52.

[28] Shannag M, Abu-Dyya N. Lateral load response of high performance fiber reinforced concrete beam-column joints. J Const Build Mat 2005;19:500–8.

[29] Liu C. Seismic behavior of beam-column joint assemblies reinforced with steel fibers. University of Canterbury; 2006. MSCE thesis.

[30] Tsonos A. Effectiveness of CFRP jackets and RC jackets in post earthquake and pre earthquake retrofitting of beam column sub-assemblages. J Eng Struct 2008;30:777–93.

[31] Supaviriyakit T, Pimanmas A. Comparative performance of a substandard beam-column joint with and without initial bond between beam bars and concrete in the joint core. Thammasat Int J Sc Tech 2007;12(1).

[32] Le-Trung K, Lee K, Lee J, Lee DH, Woo S. Experimental study of RC beam–column joints strengthened using CFRP composites. Composites B 2010;41(1):76–85.

[33] Ma C, Wang D, Wang Z. Seismic retrofitting of full-scale RC interior beam-column-slab subassemblies with CFRP wraps. Compos Struct 2017;159:397–409.

[34] Esmaeeli E, Danesh F, Tee KF, Eshghi S. A combination of GFRP sheets and steel cage for seismic strengthening of shear-deficient corner RC beam-column joints. Compos Struct 2017;159:206–19.

[35] Danesh F, Esmaeeli E, Alam M. Shear strengthening of 3D RC beam-column connection using GFRP: FEM study. Asian J Appl Sci 2008;1(3):217–27.

[36] Mosallam AS. Structural upgrade of reinforced concrete column-tie beam assembly using FRP composites. American Concrete Institute, SP-258; 2008. p. 63–74.

[37] American Society for Testing and Materials. Standard test method for tensile properties of polymer matrix composite materials. ASTM D3039/D3039M − 17ASTM international; 2017.

[38] International Code Council Evaluation Service (ICC-ES) Acceptance Criteria AC125. Acceptance criteria for concrete and reinforced and unreinforced masonry strengthening using externally bonded Fiber-Reinforced Polymer (FRP) composite systems, Brea, CA, USA; 2017.

[39] American Concrete Institute (ACI). Guide for design and construction of externally bonded FRP systems for strengthening concrete structures. ACI Committee 440; 2008.